2012

# ROMP-based thermosetting polymers from modified castor oil with various cross-linking agents

Rui Ding
*Iowa State University*

# ROMP-based thermosetting polymers from modified castor oil with various cross-linking agents

by

**Rui Ding**

A thesis submitted to the graduate faculty

in partial fulfillment of the requirements for the degree of

MASTER OF SCIENCE

Major: Materials Science and Engineering

Program of Study Committee:
Michael R. Kessler, Major Professor
Xiaoli Tan
Gap-yong Kim

Iowa State University

Ames, Iowa

2012

# Table of Contents

**Acknowledgements** ..... iii

**Abstract** ..... iv

**Chapter 1: General Introduction** ..... 1

**Chapter 2: Material Synthesis and Fabrication** ..... 11

2.1 Materials ..... 11

2.2. Synthesis of Norbornenyl-Functionalized Castor Oil Alcohol (NCA) ..... 11

2.3. Synthesis of Crosslinker ..... 14

2.4. General Sample Preparation ..... 14

2.5. Cure Processing and Specimen Fabrication ..... 16

**Chapter 3: Experimental Techniques of Characterization** ..... 18

3.1. Differential Scanning Calorimetry (DSC) ..... 18

3.2 Dynamic Mechanical Analysis (DMA) ..... 20

3.3 Swelling Test ..... 22

3.4 Tensile Test ..... 23

3.5 Thermogravimetric Analysis (TGA) ..... 23

**Chapter 4: Cure Behavior** ..... 25

4.1 Isothermal Kinetic Method ..... 25

4.2 Multiple Heating Rate Method ..... 29

**Chapter 5: Thermal Mechanical Properties** ..... 35

5.1 Glass Transition Temperature ..... 35

5.2 Dynamic Mechanical Properties ..... 39

5.3 The Evaluation of Cross-Link Density ..... 43

5.4 Tensile Properties ..... 47

5.5 Thermal Stability ..... 49

**Chapter 6: General Conclusions** ..... 53

**Reference** ..... 56

# Acknowledgements

I would express my great thanks to my advisor, Dr. Michael R. Kessler, for the opportunity to perform my graduate research in the Polymer Composites Group, and for his thoughtful guidance and encouragement throughout my study. I am sincerely appreciative to Dr. Gap-yong Kim and Dr. Xiaoli Tan for serving on my advisory committee and for their valuable views to my research activity.

I give my special gratitude to Dr. Timothy C. Mauldin, who selflessly devoted his effort and energy to instructing me during my first year. His expertise, enthusiasm, and strict attitude toward science have had a significant influence on my personal development. I would also like to thank the postdoctoral researchers and graduate students in the group for providing technical support as well as intellectual assistance. In particular, Dr. Ying Xia and visiting scholar Amir Badshah guided me on organic synthesis, Dr. Prashanth Badrinarayanan trained me on differential scanning calorimetry, Hongyu Cui supported me on dynamic mechanical analysis and tensile tests, Dr. Samy A. Madbouly assisted me on rheology tests, and Mr. Russell Hoffman collaborated with me on CNC machining. In addition, research fellows and friends Chaowei Feng, Diana Gottschalk, Eliseo De Leon, Pete Hondred, Yuzhan Li, Kunwei Liu, Hongchao Wu, Chaoqun Zhang and Zihou Zhang deserve many thanks for their cordially help, exchange of thoughts and efforts in creating a delightful working atmosphere at Iowa State University.

Deepest gratitude is dedicated to my beloved parents. No one like you will always give me support and encouragement to conquer any difficulty I meet.

# Abstract

Polymers derived from bio-renewable resources are finding an increase in global demand. In addition, polymers with distinctive functionalities are required in certain advanced fields, such as aerospace and civil engineering. In an attempt to meet both these needs, the goal of this work aims to develop a range of bio-based thermosetting matrix polymers for potential applications in multifunctional composites. Ring-opening metathesis polymerization (ROMP), which recently has been explored as a powerful method in polymer chemistry, was employed as a unique pathway to polymerize agricultural oil-based reactants.

Specifically, a novel norbornyl-functionalized castor oil alcohol (NCA) was investigated to polymerize different cross-linking agents using ROMP. The effects of incorporating dicyclopentadiene (DCPD) and a norbornene-based crosslinker (CL) were systematically evaluated with respect to curing behavior and thermal mechanical properties of the polymers. Isothermal differential scanning calorimetry (DSC) was used to investigate the conversion during cure. Dynamic DSC scans at multiple heating rates revealed conversion-dependent activation energy by Ozawa-Flynn-Wall analysis. The glass transition temperature, storage modulus, and loss modulus for NCA/DCPD and NCA/CL copolymers with different cross-linking agent loading were compared using dynamic mechanical analysis. Cross-link density was examined to explain the very different dynamic mechanical behavior. Mechanical stress-strain curves were developed through tensile test, and thermal stability of the cross-linked polymers was evaluated by

thermogravimetric analysis to further investigate the structure-property relationships in these systems.

# Chapter 1: General Introduction

Bio-based polymers and composites have been explored since the end of last century due to the increasing demand for alternatives to petroleum-based polymeric materials. Agricultural oils, such as soybean oil, corn oil, linseed oil, castor oil, and tung oil, which until then were mainly utilized in the food, painting, and coating industries are recently considered ideal biorenewable resources to synthesize bulk polymers. Although agricultural oil-based polymers envision the advantages including eco-friendliness, sustainability and low cost of feedstock, a few critical issues such as thermo-mechanical properties, durability, and weather resistance remain challenging. If these properties could be improved, the application of bio-polymeric materials derived from agricultural oils could be widely extended towards civil engineering, electronics, and other industries.

Agricultural oils, mostly extracted from vegetables and plants, are mainly triglycerides, an ester formed by one glycerol and three fatty acids. The fatty acids may vary considerably in molecular chain length and unsaturation, usually containing 14 to 22 carbon atoms, and 0 to 3 double bonds. A brief summary of fatty acid compositions in common agricultural oils is given in Table 1.1. Double bonds in triglycerides, with a high quantity or in conjugated form, make the polymerization of oil monomers relatively easy. Tung oil, contains a conjugated triene in each fatty acid chain, has been successfully polymerized through free-radical or cationic polymerization, which ranges from rubbery to tough and rigid materials by adjusting the ratio of co-monomers [1, 2]. In addition to double bonds, a variety of functional groups, such as hydroxyls, epoxies, cyclic groups,

furanoid groups exist in fatty acids of exotic oils, provide ideal active sites which are susceptible to the introduction of polymerizable groups. For the common oils without natural functionality, double bonds are used to be converted into epoxy, hydroxyl, or cyclic groups by synthetic techniques for further modification of polymerizable groups. Some successful applications in industry are epoxidized soy bean oil (ESBO), norbornenylized linseed oil (Dilulin), and dicyclopentadiene-modified linseed oil (ML189), et al.

Table 1.1 Formulas and structures of important fatty acids

| Fatty Acid | Formula | Structure |
|---|---|---|
| Caprylic | $C_8H_{16}O_2$ | 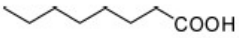 |
| Capric | $C_{10}H_{20}O_2$ | 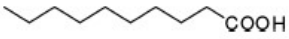 |
| Lauric | $C_{12}H_{24}O_2$ | 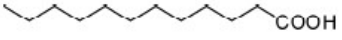 |
| Myristic | $C_{14}H_{28}O_2$ | 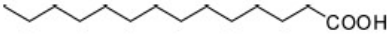 |
| Palmitic | $C_{16}H_{32}O_2$ | 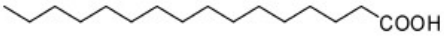 |
| Palmitoleic | $C_{16}H_{30}O_2$ | 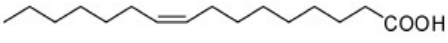 |
| Stearic | $C_{18}H_{36}O_2$ | 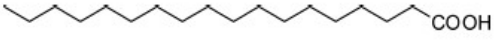 |
| Oleic | $C_{18}H_{34}O_2$ | 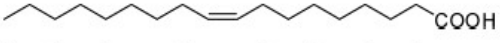 |
| Linoleic | $C_{18}H_{32}O_2$ | 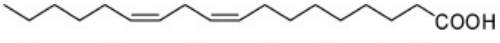 |
| Linolenic | $C_{18}H_{30}O_2$ | 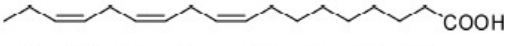 |
| α-Eleostearic | $C_{18}H_{30}O_2$ | 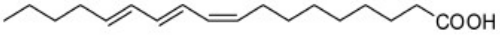 |
| Ricinoleic | $C_{18}H_{34}O_3$ | 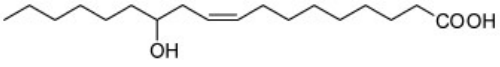 |
| Vernolic | $C_{18}H_{32}O_3$ | 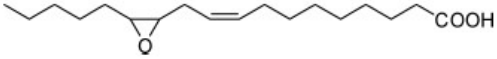 |

Triglycerides contain long and flexible branches with highly rotational features, the resulting polymers usually exhibit low glass transition temperature ($T_g$) and moduli. Many recent efforts focused on the optimization of the thermo-mechanical properties whilst exploring new agricultural oil-based polymers and its composites (also known as polymer

matrix composites). One efficient approach is to incorporate commercial comonomers with rigid chemical structure into the polymers. R. Wool [3] used a blend of styrene with acrylated epoxidized soybean oil (AESO) and soybean oil monoglyceride (SOMG) maleates, respectively, which increased the degree of free-radical polymerization and the storage modulus ($E'$) at room temperature. Dicyclopentadiene (DCPD) was first used by M. Kessler, R. Larock et al [4-8] as an additive component in cationic polymerization and in ring-opening metathesis polymerization (ROMP) of modified linseed oil. The observed increase in both $T_g$ and $E'$ was attributed to the rigid cyclopentane groups resulting from polymerization. Another approach to enhancing mechanical properties is to increase the degree of cross-linking in the network. One route is to multiply the average number of reactive sites in the triglycerides. The increased hydroxyl functionalities for each fatty chain can be achieved by reactions such as glycerolysis, amidation, methanolysis, or ester reduction, which were reported significantly improved certain thermo-mechanical properties [9-11]. The addition of multifunctional agents is also considered an efficient route at present though it compromise part of biorenewable purpose. Divinylbenzene, and norbornene-based cross-linking agents (as also called crosslinkers in ROMP studies), are frequently used to increase thermo-mechanical properties [12-15]. Other low molecular weight agents such as maleic acid, cyclohexane dicarboxylic acid may also provide more cross-linked sites as well as rigid cyclic groups to stiffen the bio-based polymers.

Ring-opening metathesis polymerization (ROMP) is a relatively new-emerged technique of synthesizing macromolecules in the field of polymer chemistry. It was first

recognized in the mid-1950s when studying olefin metathesis by exploring various metal initiators and reagents. because of its unique reaction pathway, today ROMP has become a powerful method that enables a wide range of polymers with complex architectures and useful functions [16].

ROMP was discovered from unexpected results through a Ziegler-Natta-type polymerization: norbornene and cyclopentene was polymerized to ring-opened, unsaturated polymers when using alternate metal initiators. A general ROMP mechanism is shown in Figure 1.1:

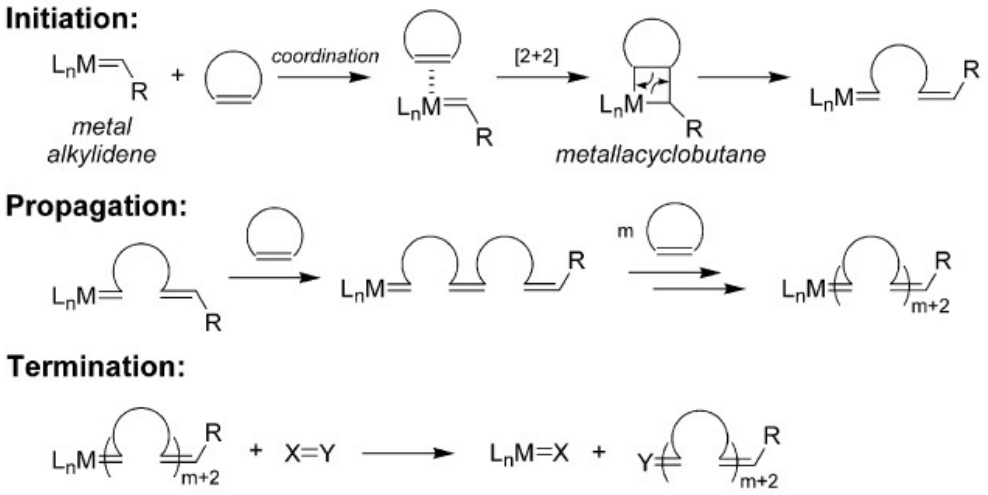


Fig.1.1 A general mechanism of ROMP based on metal carbene (alkylidene) complexes

In the initiation stage, the transition metal alkylidene complex coordinates to one cyclic olefin and subsequently forms a 4-membered metallacyclobutane intermediate through [2+2]-cycloaddition. The following cycloreversion reaction generates a new metal alkylidene. The resulting complex retains almost the same reactivity toward cyclic olefins as it grows longer with every repetition of the first step. The continuous

consumption of cyclic olefins during chain growth is identified as the propagation step. The polymerization is terminated when the monomer is totally depleted or when the transition metal is deactivated or removed. With these characteristics, ROMP represents a type of chain-growth polymerization process based on olefin metathesis, a unique metal-mediated carbon-carbon double bond exchange process [17].

The driving force for ROMP is the release of ring-strain in cyclic olefins. Therefore, monomers with a high degree of strain (> 5 kcal/mol), such as cyclobutene, cyclopentene, cis-cyclooctene, and norbornene and their derivatives are ideal candidates for ROMP [18]. Similar to other polymerization mechanisms, several side reactions compete with ROMP. These secondary metathesis reactions include intermolecular chain-transfer, which results in the distribution of molecular weight of individual polymers, and intramolecular chain-transfer, also called backbiting, produces macro-cyclic polymer chains with reduced molecular weight [19].

A comprehensive understanding of ROMP mechanism gives rise to the exploration of well-defined metathesis catalysts for manipulation requirement. In recent decades, the late transition metal ruthenium has been intensively investigated as a ROMP catalyst [20]. Ruthenium catalysts offer a range of advantages over the early catalysts: they are air and moisture stable, solvent compatible, functional group tolerant, and highly reactive, which enables this catalyst family to carry out living polymerization and prepare numerous block-, graft-, branch-copolymers and end-functionalized polymers [21]. The ruthenium-based carbene initiators are better-known as Grubbs' catalysts, named after the

laureate of 2005 Nobel Prize in chemistry [22]. The most popular Grubbs' catalysts in application to date are categorized in Figure 1.2 :

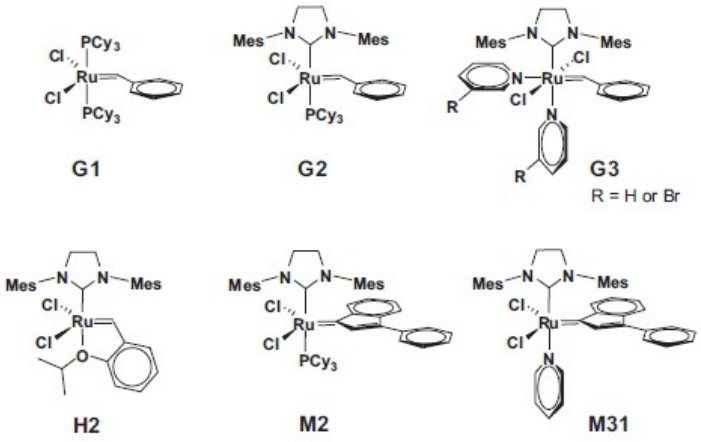


Fig. 1.2 Family of Grubbs' catalysts

Some linear polymers and thermosets important for industrial applications are readily produced via ROMP [23-25]. Some examples of the commercial polymers are Vestenamer (or trans-polyoctenamer), which is synthesized from cyclooctene; Norsorex is the ROMP product of norbornene; Telene and Metton are polydicyclopentadienes, another critical ROMP polymer on the market.

In addition to the current industrial applications, ROMP has also shown great potential in the cutting-edge field of self-healing materials (illustrated in Figure 1.3) .

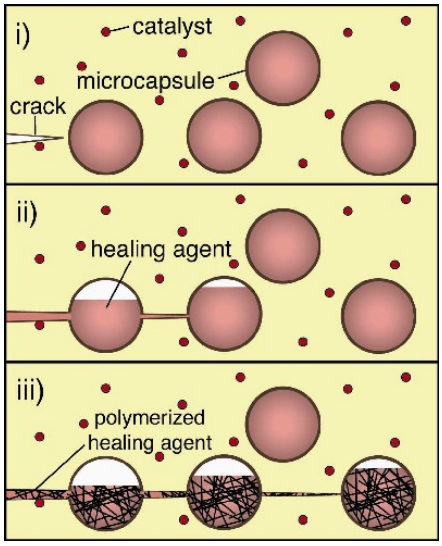


Fig.1.3 Concept of self-healing using microencapsulated healing agents and ROMP initiators

The first reported self-healing system consisted of microencapsulated endo-dicyclopentadiene (DCPD) as the healing agent and 1$^{st}$ generation Grubbs' catalyst (shown as G1 in Figure 1.2) as the ROMP initiator, distributed in an epoxy matrix [26]. To improve the autonomic repairing performance of microcapsule-style self-healing systems, extensive work has been done by our research group on the optimization of ROMP-based healing agent/catalyst combinations. 5-Ethylidene-2-norbornene (ENB) and *exo*-isomer of DCPD were investigated and it was determined that they exhibit higher ROMP reactivity than endo-DCPD in bulk polymerization [27-30]. Catalyst dissolution kinetics was studied to optimize selection of ROMP monomers that can be rapidly dissolved and provide better healing performance [31]. Besides, a mimic evaluation of self-healing kinetics was carried out by a modified rheokinetic technique [32]. Efforts were also concentrated on improving the mechanical properties of ROM polymerized healing agents. For example, the addition of norbornene-based cross-linking agents

increased storage modulus, glass transition temperature, and cross-linking density of the resulting thermosets [33, 34]. In addition, chemical modification allowed for good dispersion of multi-walled carbon nanotubes (MWNT) in DCPD or ENB that were subsequently ROMP-cured into uniform composites. The system displayed exciting significant increase in toughness and in strain to failure, even at very low filler loadings (< 5 wt.%) [35, 36].

Recently, the application of ROMP techniques provides a new horizon in the development of well-performing thermosets from vegetable oils. Ruthenium-based catalysts proved to successfully initiate ROMP of oil-derivative monomers due to their high reactivity, functional group tolerance, and air/moisture insensitivity. Dilulin [37], a commercially available linseed oil that is modified with cyclopentadiene, was copolymerized with DCPD (crosslinker) by ROMP. However, the low number of strained rings ( about one ring per triglyceride) in Dilulin [4] reduced the efficiency of network formation. The oligomer content also had a plasticizing effect that lowered the mechanical strength. Xia [9] synthesized a norbornene-modified fatty alcohol from soybean oil (NMDA) using Dilulin as a base structure, which was characterized that one third of the fatty chains were appended with two norbornene groups. DMA results showed that the pure polyNMDA exhibited $E'$ of 590 MPa at room temperature, $T_g$ of 66.5$^{o}$C, presenting an significant progress in thermo-mechanical properties. Copolymer systems from norbornene-functionalized castor oil and castor oil alcohol (polyNCO/NCA) [10] were developed to overcome the processing problems caused by the relatively high

viscosity of norbornene-modified castor oil alcohol (NMCA). This approach also increased the number of norbornyl functionality to approx. 1.7 per fatty chain. Neat thermosetting NCA resin polymerized via ROMP exhibited relatively fast gelation times, high value of $T_g$, modulus, tensile strength and high cross-link density compared to its predecessors.

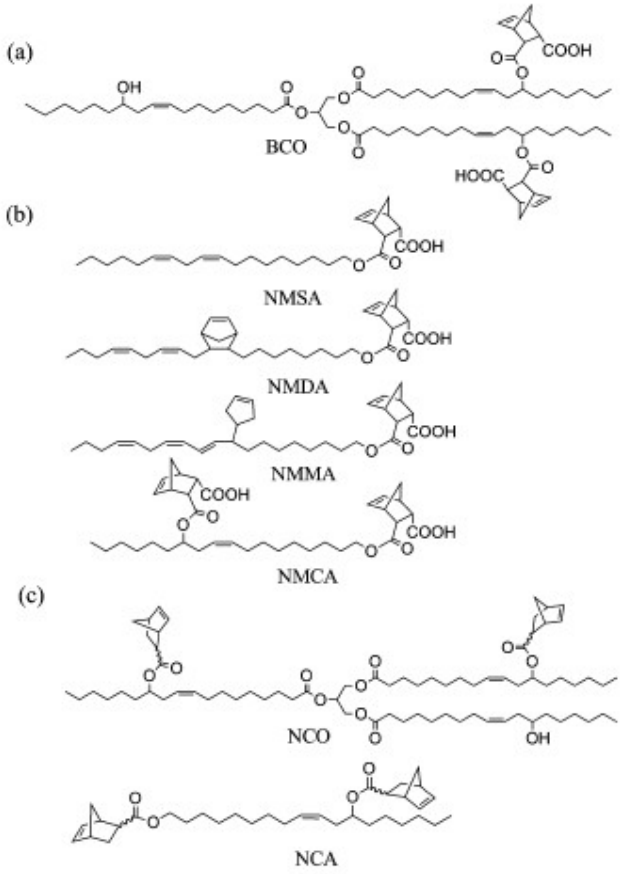


Fig. 1.4 ROMP-active monomers from agricultural oil;
(a)bicyclic castor oil derivative (BCO), (b) norbornene-modified fatty alcohol from soybean oil (NMSA), Dilulin (NMDA), ML189 (NMMA), and castor oil (NMCA) (c) norbornene-functionalized castor oil (NCO), and norbornene-functionalized castor oil alcohol (NCA)

In this work, we investigated how the cure behavior and thermo-mechanical

properties can be tailored by ring-opening metathesis co-polymerization of norbornyl-functionalized castor oil alcohol (NCA) with multifunctional co-monomers, DCPD, and crosslinker [4, 13, 38]. Differential scanning calorimetry (DSC) was performed using isothermal kinetic method to investigate the influence of the two cross-linking agents on the conversion and the conversion rate during cure. Dynamic scans with multiple heating rates revealed the evolution of activation energy at different curing levels by Ozawa-Flynn-Wall isoconversional analysis. Dynamic mechanical properties of the resulting copolymers were studied via dynamic mechanical analysis (DMA), such as glass transition temperature, storage modulus, loss modulus and loss tangent. Mechanical properties and thermal stability, respectively, were compared using tensile tests and thermogravimetric analysis (TGA) at various loading levels of cross-linking agents. The effect of cross-linking and structural rigidity was evaluated to explain the divergence in behavior between systems.

# Chapter 2: Material Synthesis and Fabrication

## 2.1 Materials

The following chemicals were used in the synthesis of norbornenyl-functionalized castor oil alcohol (NCA): castor oil, lithium aluminum hydride (LAH) (95 %), 5-norbornene-2-carboxylic acid (98 %, a mixture of *endo*- and *exo*-, predominantly *endo*), thionyl chloride (99.5 %), triethylamine (TEA). All were obtained from Sigma-Aldrich. Tetrahydrofuran (THF)(HPLC), ethyl acetate, methylene chloride ($CH_2Cl_2$), anhydrous magnesium sulfate ($MgSO_4$), sodium hydroxide (NaOH), sodium carbonate ($Na_2CO_3$), and hydrochloric acid (HCl) were supplied by Fisher Scientific. THF was refluxed over sodium/benzophenone under $N_2$ and distilled for immediate use. The same purification steps were applied for $CH_2Cl_2$ with $CaH_2$.

The chemicals used for the preparation of the cross-linking agent (CL) were: dicyclopentadiene, bicyclo[2.2.1]hepta-2,5-diene, hydroquinone; all were purchased from Sigma-Aldrich.

2$^{nd}$ generation Grubbs' catalyst [1,3-bis-(2,4,6-trimethylphenyl)-2-imidazolidinyl idene]dichloro(phenylmethylene)(tricyclohexylphosphine)ruthenium] was supplied by Sigma-Aldrich. Benzene was supplied by EMD Chemicals Inc.

## 2.2. Synthesis of Norbornenyl-Functionalized Castor Oil Alcohol (NCA)

The preparation of NCA included three major steps illustrated in Figure 2.1. The synthesis of the ROMP-reactive functionalizing agent bicyclo[2.2.1]hept-2-ene-5-

carbonyl chloride was a modified approach cited in [39].

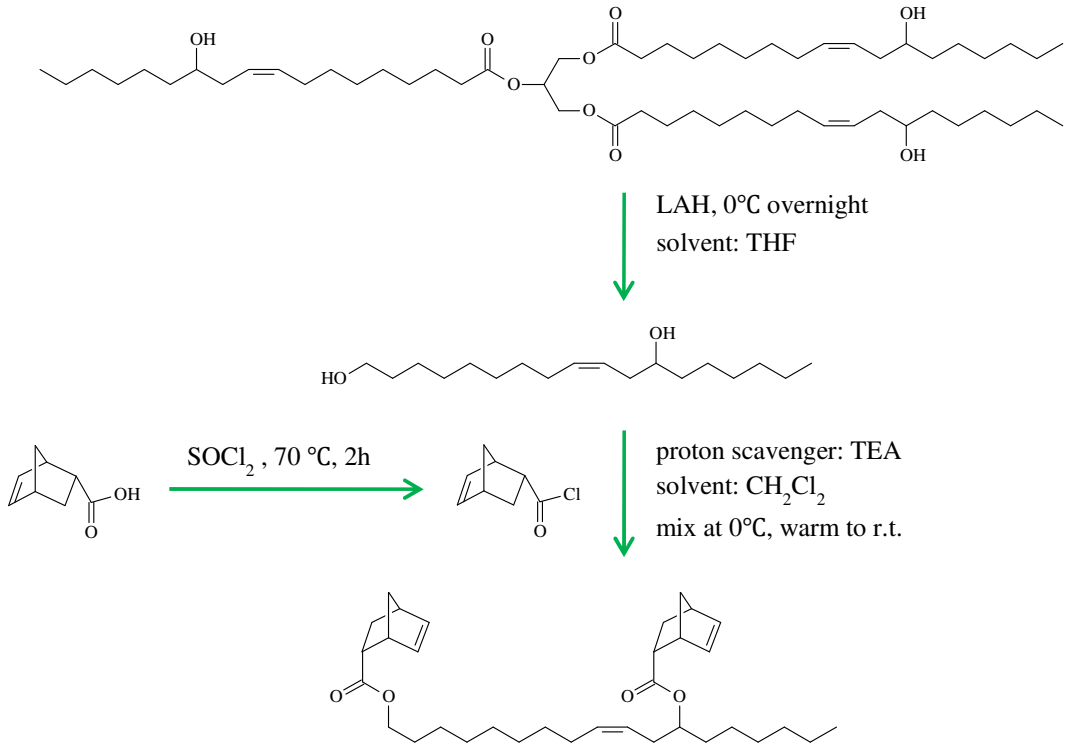


Fig.2.1 Reaction scheme of synthesizing NCA

The carbonyl chloride was prepared by refluxing a mixture of *endo*- and *exo*-bicyclo[2.2.1]-hept-5-en-2-carboxylic acid (25.0 g, 0.204 mol) and thionyl chloride (30 mL, 0.408 mol) for 3 h under $N_2$. The residual $SOCl_2$ was removed under reduced pressure distillation at 0.5 Torr at 42 $^{o}$C. The crude product was purified by redistillation and resulted in a colorless liquid of 70 % yield. $^{1}$H-NMR ($CDCl_3$, d ppm) at 1.32-1.34 (d), 1.47-1.52 (m), 1.92-1.98 (m), 2.00-2.05(m), 2.72-2.76 (m), 2.99 (s), 3.29 (s), and 3.43-3.47 (m) were assigned to the non-olefinic protons of both the *endo* and *exo* isomers; 6.02-6.04 (m,=CH, endo), 6.11-6.14 (m,=CH, exo), 6.20-6.22 (m, =CH, exo), 6.25-6.27

(m, =CH, endo). The molar ratio of *endo* isomer to *exo* isomer was about 74:26.

The preparation of NCA from castor oil followed the method reported by [40]:

LAH (12.27 g, 0.32 mol) was added to 100 mL of THF and stirred in a 1000 mL two-neck round bottom flask at 0 $^{o}$C. Castor oil (100 g, 0.11 mol) was dissolved in 600 mL of THF and then added dropwise to the LAH suspension. The reaction was maintained at 0 $^{o}$C overnight. The reaction mixture was poured into ice water, followed by the addition of 1 M HCl, until the solution was clear. Then 300 mL of ethyl acetate was added to carry out the extraction. The organic layer was washed with water to remove glycerol, dried over $MgSO_4$ and filtered. Finally, the clear castor oil alcohol was obtained after removal of the organic solvent under vacuum.

Castor oil alcohol (20 g, 0.071 mol) was dissolved in 100 mL of anhydrous $CH_2Cl_2$ and cooled to 0 $^{o}$C. A solution of bicyclo [2.2.1] hept-2-ene-5-carbonyl chloride (22.73 g, 0.15 mol) in 100 mL of anhydrous $CH_2Cl_2$ was added drop wise and then triethylamine (14.68 g, 0.15 mol) was added. The solution was stirred, while allowing it to warm from 0 $^{o}$C to room temperature, and was maintained for 24 h at that temperature. Then the reaction mixture was stirred with 500 mL of aqueous 5 wt% $Na_2CO_3$ solution overnight to convert the excess bicyclo[2.2.1]hept-2-ene-5-carbonyl chloride to a water soluble

carboxylate salt. After extraction with $CH_2Cl_2$ and removal of the solvent, a quantitative yield of NCA with a light brown color was obtained.

## 2.3. Synthesis of Crosslinker

The norbornene-based crosslinker (CL) was a mixture of 1,4,4a,5,8,8a-hexahydro -1,4,5,8-exo,-endo-dimethanonaphthalene (*exo-, endo*-CL) and 1,4,4a,5,8,8a-hexahydro-1,4,5,8-endo,-endo-dimethanonaphthalene (*endo-, endo*-CL), which is described by the formula $C_{12}H_{14}$. The synthesis procedure described here refers to work by [38].

Bicyclo[2.2.1] hepta-2,5-diene (8.6 g, 93.3 mmol) and hydroquinone (13 mg, 0.12 mmol) were added to endo-dicyclopentadiene (6.2 g, 46.9 mmol) in a hard-glass pressure vessel. After the vessel was tightly sealed, the mixture was heated to react at 190 $^{o}$C for 18 h. The resulting product was subjected to fractional distillation under reduced pressure, which yielded a clear liquid (7.8 g, 52.9%). The fraction of exo-, endo- isomer, and *endo-, endo*-isomer was 83%:17%.

## 2.4. General Sample Preparation

In this study, NCA resin was mixed with either DCPD or CL at various loading levels: 10, 20, 30, 50 wt.% by comonomer. Because the melting point of DCPD is at 33 $^{o}$C, all samples were placed in an oven at 70 $^{o}$C for 5 min and then dispersed to form a homogeneous solution. 10 grams of each sample were prepared for the subsequent experiments: the freshly catalyzed resin was withdrawn by a few amount for cure kinetics (described in Section 3.1) in priority and the rest were fully cured in a mold for thermal

and mechanical analysis (described in Section 3.2).

Before the ruthenium catalyst was added to trigger the ROMP reaction, it was routinely freeze-dried in order to enhance its solubility in the monomer [41]. The 2nd generation Grubbs' catalyst (100 mg) was dissolved in 2 mL of benzene in a small vial and then flash-frozen in a liquid nitrogen bath. The frozen solution was vacuumed in an ice bath for 5 h to sublime the benzene. The process was repeated when larger amounts of catalyst were needed.

The catalyst was dissolved very carefully to minimize undesired reactions of the uncured resins in later DSC tests. The weighed freeze-dried catalyst (12.5 mg, 0.125 wt.%) was added to the resin mixture, which had been cooled to 0 $^{o}$C in advance. The mixture was then agitated vigorously with a spatula for 10 s until it was assured that the catalyst was completely dissolved. The ROMP reaction scheme of NCA with cross-linking agents is illustrated in Figure 2.2.

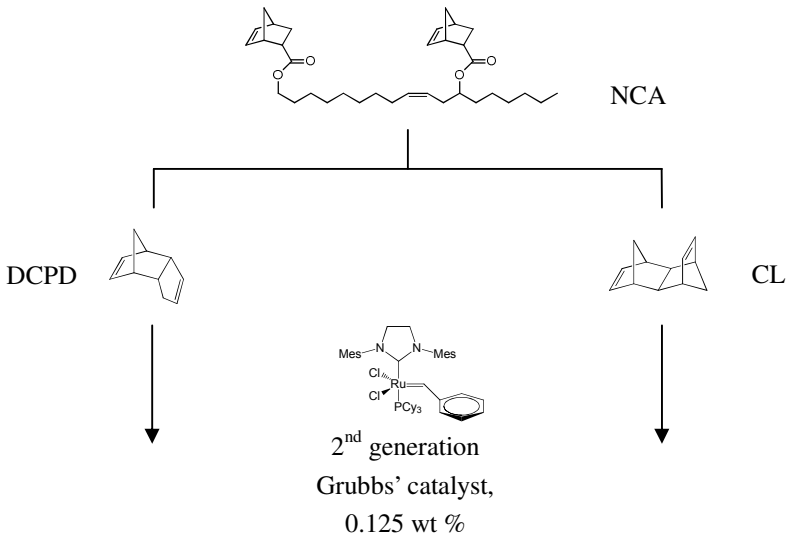

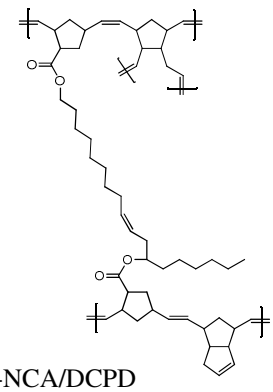

poly-NCA/DCPD

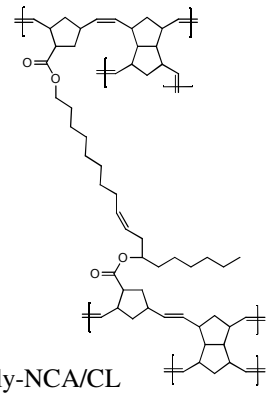

poly-NCA/CL

Fig. 2.2 ROMP reaction scheme of NCA with cross-linking agents

## 2.5. Cure Processing and Specimen Fabrication

The solution was injected into a glass mold, first cured at 60 $^{o}$C for 1.5 h and then post-cured at 135 $^{o}$C for 12 h. The resulting thermosets were transparent but retained the monomers' original color.

Soxhlet extraction was performed as follows: a 1.5 g sample of the bulk polymer was extracted for 24 h with 100 mL of refluxing methylene chloride using a Soxhlet extractor. Following extraction, the resulting solution was concentrated under reduced pressure and dried in a vacuum oven at 60 $^{o}$C overnight

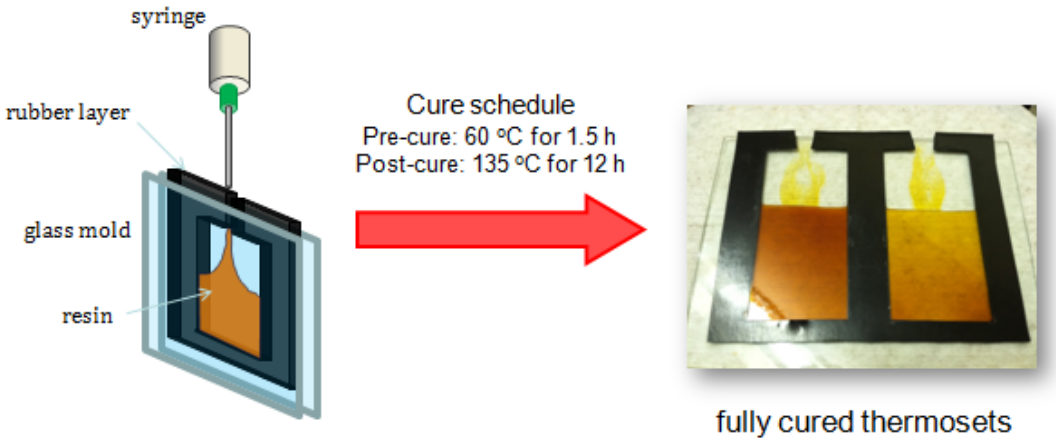


Fig. 2.3 Schematic of resin injection molding and cure schedule

# Chapter 3: Experimental Techniques of Characterization

## 3.1. Differential Scanning Calorimetry (DSC)

Differential Scanning Calorimeter (DSC), emerging after differential temperature analyzer (DTA), is a powerful tool to collect vital information of materials with respect to temperature, such as physical transitions and chemical reactions. According to ASTM, DSC is defined as a technique that measures the difference in heat flow rate between a substance and a reference as a function of temperature or time. Polymer is a major field where DSC technique is widely applied. Common applications include: (1) the fast determination of glass transition temperature, melting and crystallization, and even liquid crystal transitions; (2) quantitative measurements such as heat of fusion, heat of reaction, heat capacity; (3) kinetic evaluation of chemical reactions such as curing, thermal and thermooxdative degradation.

Using DSC to study cure kinetics is a routine procedure for the characterization of a new thermosetting resin. Cure kinetics provide indispensable information for the processing of thermosets because we want to manipulate how fast and what condition of cure reaches before the cross-linked polymer network forms in shape. Typically, cure characterization involves the following measurements: the heat of reaction, the degree and rate of conversion, $T_g$, and characteristic cure parameters. Other critical cure behaviors, such as gelation and vitrification, can be detected by rheology, DMA, or MTDSC.

In the following, the cure behavior of castor oil-based thermosetting resins blended

with ROMP co-monomers is investigated by DSC using both isothermal kinetic method and multiple heating rate method. With the isothermal kinetic method, the cure reaction proceeds at a constant temperature over time while both the conversion and the rate of conversion are continuously monitored. Multiple heating rate method allows to measure the change of activation energy versus temperature where constant conversion reaches.

For DSC measurements, samples with different compositions were prepared immediately after the step of dissolving the catalyst into the resin blends (described in Section 2.4). A syringe was used to draw in some liquid, then quickly squeeze it drop wise into liquid nitrogen. Thus, the catalyzed resin was flash-frozen into glassy beads and any unwanted reactions were prevented before measurements took place. Also, this procedure conveniently provided the desired sample size of approx. 5-10 mg. The beads of uncured resin were weighed and sealed in Tzero hermetic pans immediately prior to starting a scan.

Q2000 and Q20 differential scanning calorimeters (TA instruments, Inc.) were used to test the cycles of isothermal and dynamic curing, respectively. First, a dynamic scan from -100 $^{o}$C to 200 $^{o}$C at a heating rate of 20 $^{o}$C/min was tested with a NCA-comonomer sample. The obtained thermogram provided preliminary information regarding the temperature range of the exothermal peak, which assisted in the subsequent test set-up.

For the isothermal kinetic DSC method, a Tzero pan with a weighed sample (~ 9 mg) inside was loaded into the DSC cell at a standby temperature of -50 $^{o}$C. After thermal equilibration for 1 min, the DSC cell was fast heated to the required temperature ($T_c$ = 50,

60, 70 $^{o}$C) at a heating rate of 100 $^{o}$C/min. Next, the cell was isothermally soaked at the cure temperature for 1 h. After that, the program was set to ramp down to -50 $^{o}$C at a rate of 10$^{o}$C/min, followed by a dynamic scan ramping up to 250 $^{o}$C at a rate of 10 $^{o}$C/min. The second scan is purposed to measure the residue reaction heat as well as the final conversion under isothermal cure conditions. For all isothermal experiments, helium gas was purged through the DSC cell at a constant flow rate of 25 mL min$^{-1}$.

Five different heating rates (1, 2, 5, 10, 20 $^{o}$C/min) were chosen for dynamic scanning utilizing the multiple heating rate method. Measurements were not performed until the DSC chamber was cooled down to -100 $^{o}$C and finished at 200 $^{o}$C.

## 3.2 Dynamic Mechanical Analysis (DMA)

Dynamic mechanical techniques, which are often referred to DMA, are the most popular methods to study the viscoelastic properties of both polymeric solids and liquids. DMA involves applying a small sinusoidal strain to a sample and measuring the resulting stress. Polymeric material's characteristic viscoelasticity is described by the stress-strain response in the form of complex modulus, which is defined as:

$$E^* = E' + iE''$$

$$E' = \frac{\sigma_0}{\varepsilon_0}\cos(\delta), \quad E'' = \frac{\sigma_0}{\varepsilon_0}\sin(\delta) \tag{3.1}$$

$E'$ is known as the storage modulus, which measures the elastic character of the material, while $E''$ is known as the loss modulus, which measures the viscous character of the material. $E'$ reflects the stiffness and $E''$ is related to the damping capacity of the material. The ratio of loss modulus to storage modulus is determined as the loss tangent:

$$\tan\delta = \frac{\sin(\delta)}{\cos(\delta)} = \frac{E''}{E'} \tag{3.2}$$

The loss tangent tan $\delta$ represents the ratio of energy dissipated to energy stored during the cycle of deformation. By the principle of time-temperature equivalence, we are able to observe a wide range of viscoelastic behavior with a temperature scan other than a frequency scan. A typical DMA measurement sweeping temperature with constant frequency is illustrated in Figure 3.1. The primary applications of DMA are the study of molecular relaxation processes in polymers and the determination of inherent mechanical or flow properties as a function of time and temperature. In more detail, DMA characterization includes the detection of viscoelastic transitions or relaxations such as glass transition and secondary transition, the determination of mechanical properties such as mechanical stiffness and damping, structure-property or morphology relationships, such as the effect of crystallinity, molecular weight, cross-linking, phase separation, aging, curing, orientation, additives, composites, and others.

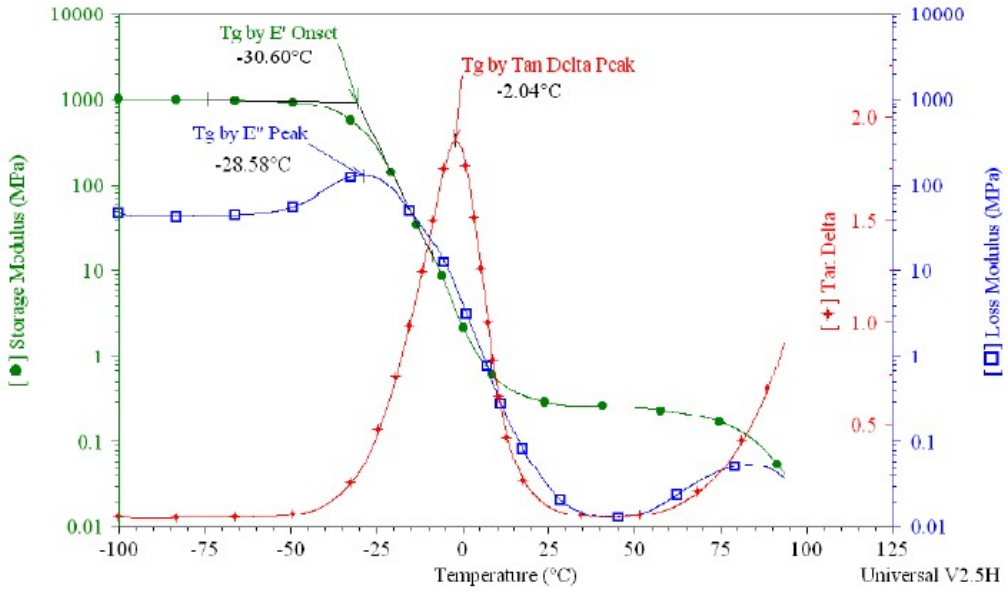


Fig. 3.1 Typical DMA plot of a polymer illustrating storage modulus, loss modulus, loss tangent and the determination of glass transition temperature

A Q800 from TA Instruments Inc. was used for DMA analysis of the full cured copolymers. Based on the geometry of thin film determined by the applied molding technique, the clamp of tension film is selected to deform specimens in test. Tests were performed as uniaxial oscillation at a constant frequency of 1 Hz and amplitude of 15 μm. Rectangular samples were die-cut with average dimension of 0.80 mm × 4.27 mm × 20.80 mm (thickness × width × length) measured between clamps. The samples were measured in a temperature range from -50 $^{o}$C to 200 $^{o}$C at a heating rate of 3 $^{o}$C /min.

## 3.3 Swelling Test

A swelling test was performed to qualitatively evaluate the cross-link density. Fully cured NCA/DCPD and NCA/CL copolymer samples were cut into small rectangular pieces (1 × 10 × 20 mm) with initial weights of $W_{initial}$. Next, the weighed samples were

soaked in methylene chloride at room temperature for 48 h. Finally, the samples were taken out and immediately weighed to determine their final weight, $W_{final}$, which included the mass of the solvent absorbed. Swelling percentage was calculated by Equation 3.3 below and is plotted as a function of cross-linker loading in Figure 5.4.

$$Swelling(\%) = \frac{W_{final} - W_{initial}}{W_{initial}} \times 100\% \tag{3.3}$$

## 3.4 Tensile Test

The mechanical properties of the thermosets were determined using an Instron universal testing machine (model 4502) with a crosshead speed of 2 mm/min. Dogbone-shaped type V specimens were milled according to ASTM D 638-03 using a CNC machine. An average value of four replicates of each sample was taken for measurement. The toughness of the polymer, which was defined as the fracture energy per unit volume of the sample, was obtained from the area under the corresponding tensile stress-strain curves.

## 3.5 Thermogravimetric Analysis (TGA)

Thermogravimetric analysis (TGA) is a widely used technique for polymer characterization where the mass of the sample is measured as a function of temperature or time while the polymer is heated following a controlled temperature program in a controlled atmosphere. The atmosphere can be created by a purge gas flowing according to the requirement, either inert or oxidizing. Mass loss in the polymer sample is often explained by loss of volatile components, reaction products, and generation of volatile

degradation products. Data regarding mass loss process obtained from TGA is useful to characterize a polymer's thermal stability, composition, and extent of cure. Kinetic analyses are also performed for modeling and prediction.

In this study, the thermal stability of NCA/DCPD and NCA/CL copolymers in oxidizing atmosphere were investigated by TGA on a TA Instruments Q50. Dynamic experiments of degradation were carried out for all copolymers. Samples were prepared into small pieces of similar size from the bulk materials and weighed approx. 10 mg for each test. TGA measurements were programmed to scan from ambient to 700 $^{o}$C at a heating rate of 20 $^{o}$C /min in air.

# Chapter 4: Cure Behavior

## 4.1 Isothermal Kinetic Method

As mentioned in Section 3.1, isothermal kinetic DSC was performed at three cure temperatures: 50, 60, and 70 °C for NCA resins blended with DCPD or CL at a 50/50 mass ratio. Figures 4.1(a) and 4.1(b) show the beginning stages of isothermal cure where exothermic peaks occurred for the respective samples. The three temperature profiles were selected based on exotherm onset temperatures for the respective composition variations in the first dynamic scan, which ranged from 67 °C to 75 °C (Here only DSC dynamic scans of NCA-DCPD resin in 50/50 mass ratio were shown in Figure 4.3).

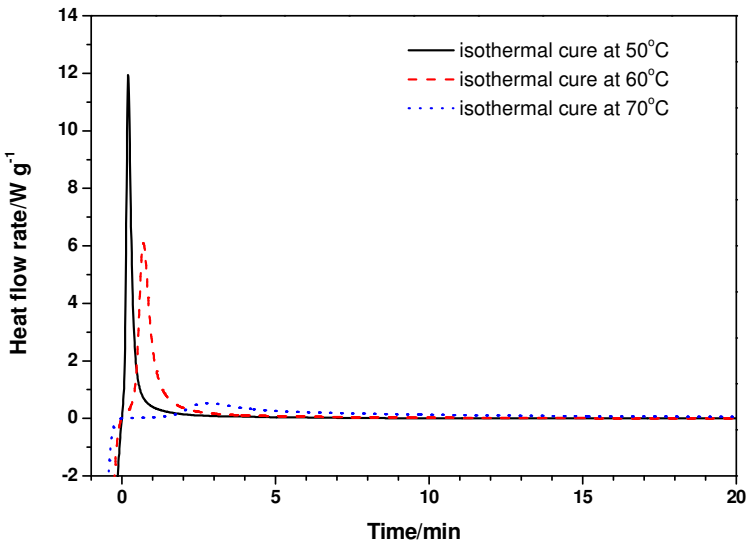


(a)

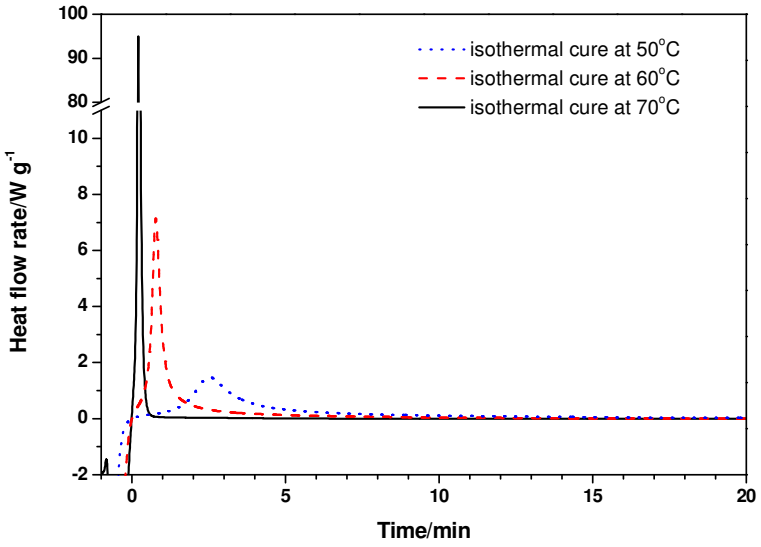


(b)

Fig. 4.1 DSC isothermal kinetic method of (a) NCA50-DCPD50 and (b) NCA50-CL50 at three curing temperatures

Conversion α, or degree of cure, is defined as:

$$\alpha = \frac{\Delta H_t}{\Delta H_{rxn}} \tag{4.1}$$

Where $\Delta H_t$ is the heat generated up to time $t$ during the cure reaction. $\Delta H_{rxn}$ is the total reaction heat per unit (J/g) from uncured (α = 0) to fully cured (α = 1). The equation is eligible only under the assumption that $\Delta H_t$ measured by DSC at instant given time is proportional to the amount of resin monomers cured.

The rate of conversion can therefore be derived by differentiation:

$$\frac{d\alpha}{dt} = \frac{dH/dt}{\Delta H_{rxn}} \tag{4.2}$$

Where $dH/dt$ represents the heat flow rate that can be directly detected by DSC. With Equation 4.2, the relationship between conversion and time can be determined by

integrating the heat flow rate. The total reaction heat $\Delta H_{rxn}$ is calculated by adding the exothermic heat generated isothermally to the residual heat scanned dynamically.

The NCA/DCDP and NCA/CL blends showed the similar time where the maximum heat flow rate or conversion rate appears. For both resins, the time for maximum conversion rate reduced significantly from about 2.5 min to about 12 s when the cure temperature was raised from 50 $^{o}$C to 70 $^{o}$C. The appearance of exothermic peaks at low conversion rather than at the starting point indicated that the isothermal cure of NCA resins is autocatalytic, which agrees with previous ROMP-based cure kinetics studies [42]. A great jump can also be seen in the value of maximum conversion rate at different temperatures, exhibiting that the isothermal cure temperature has a remarkable influence on cure kinetics. Compared to NCA-DCPD, NCA-CL resin exhibits slightly shorter conversion times as well as a higher value of the maximum conversion rate, indicating that the ROMP curing reactions of NCA/CL blends are faster than those of NCA/DCPD blends.

Figure 4.2(a) and 4.2(b) show the evolution of conversion vs. time under isothermal cure conditions for NCA50-DCPD50 and NCA50-CL50, respectively. The final conversion obtained after one-hour isothermal cure is shown in Table 4.1. At 70 $^{o}$C (the highest cure temperature), 90 % of NCA-DCPD monomers were converted into a solid network in only 5 min, and NCA-CL reacted even faster. Also, the data of final conversion indicate that a post-cure process, at which the temperature should be above $T_{g\infty}$ (glass transition temperature in the fully cured state), is necessary to complete the

residual reaction. The post-cure process is especially important for the bulk manufacture of thermosets because of their poor thermal transmission properties.

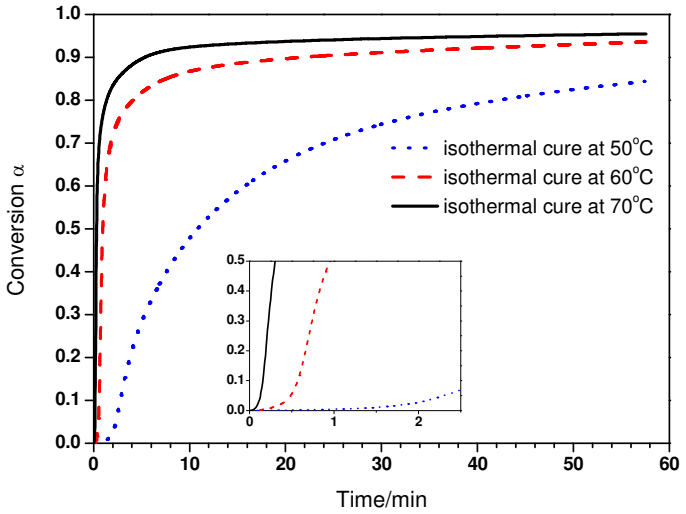


(a)

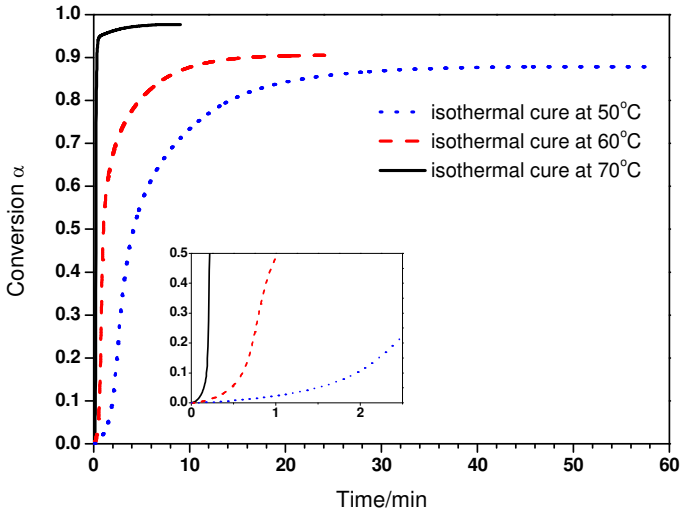


(b)

Fig. 4.2 Conversion as a function of time of (a) NCA50-DCPD50 and (b) NCA50-CL50 under isothermal cure at three curing temperatures

Table 4.1 Selected isothermal cure data from Fig. 4.1 and Fig. 4.2

| Composition | Cure temperature ($T_c$/°C) | Time of (d*H*/d*t*) max (s) | (d*H*/d*t*) max (W/g) | Final conversion α (%) |
|---|---|---|---|---|
| NCA50-DCPD50 | 50 | 12.3 | 0.53 | 84.4 |
| | 60 | 42.0 | 6.10 | 93.6 |
| | 70 | 168.6 | 11.95 | 95.5 |
| NCA50-CL50 | 50 | 12.5 | 1.47 | 87.8 |
| | 60 | 46.5 | 7.14 | 90.5 |
| | 70 | 150.7 | 95.03 | 97.7 |

Consequently, a cure schedule (described in Section 2.5) was designed to fabricate bulk specimens for NCA resins with various levels of DCPD or CL loading. For this cure schedule, 60 °C was chosen as the cure temperature for all compositions because it provides mild cure conditions for resins with high comonomer loading levels while ensuring high conversion rates for compositions with low comonomer loading. Post-curing for 12 hours at 135 °C guaranteed completion of cure reaction and prevented thermal degradation.

## 4.2 Multiple Heating Rate Method

Figure 4.3 shows typical DSC dynamic scanning curves for NCA-DCPD resins with DCPD loading varying from 0 to 50 %, at a heating rate of 20 °C/min. Every single dynamic curve shows one broad endothermic peak at approx. - 40 °C, which marks melting of the resin mixtures from the frozen state.

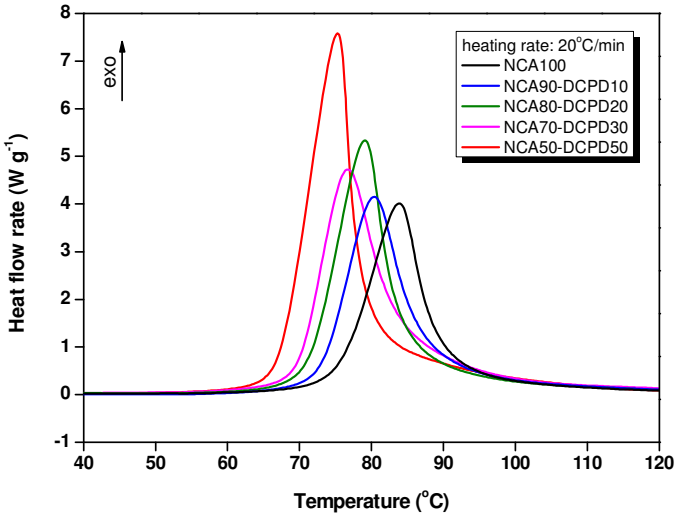


Fig.4.3 DSC dynamic scanning curves of NCA-DCPD with different mass ratios

Table 4.2 Selected dynamic scan data of NCA-DCPD resins from Fig.4.3

| Composition of NCA-DCPD | Onset temperature (°C) | Maximum temperature (°C) | Total reaction heat $\Delta H_{rxn}$ (J/g) |
|---|---|---|---|
| 100-0 | 75.42 | 83.80 | 141.7 |
| 90-10 | 72.76 | 80.42 | 156.8 |
| 80-20 | 71.10 | 79.00 | 176.4 |
| 70-30 | 69.67 | 76.77 | 187.1 |
| 50-50 | 67.16 | 75.29 | 230.2 |

DSC dynamic scans for NCA50-DCPD50 and NCA50-CL50 resin at heating rates of 1, 2, 5, 10, and 20 °C/min are shown in Figure 4.4(a) and 4.5(a), respectively. All experimental thermograms were normalized with regards to the heating rate. As can be seen, only one single exothermic peak appeared on the thermogram corresponding to each heating rate. The uniform distribution of peaks indicates a diminished heterogeneous reaction between oil-based monomer and commercial comonomers compared to a previous combination of Dilulin and CL [43]. The ROMP reactivity of NCA presents to

be close to DCPD and CL, which were investigated as suitable candidates of self-healing agents for their fast curing nature. As expected, the position of the exothermic peaks for both resin blends shifts to higher temperatures with increasing heating rate, and the exothermic effect is greater as well. The total reaction heat $\Delta H_{rxn}$ of NCA50-CL50 (305.9 ± 10.6 J/g) is larger than the one of NCA50-DCPD50 (238.8 ± 18.5 J/g). In addition, Table 4.2 shows that more enthalpy is released during the cure for resins with higher comonomer loading.

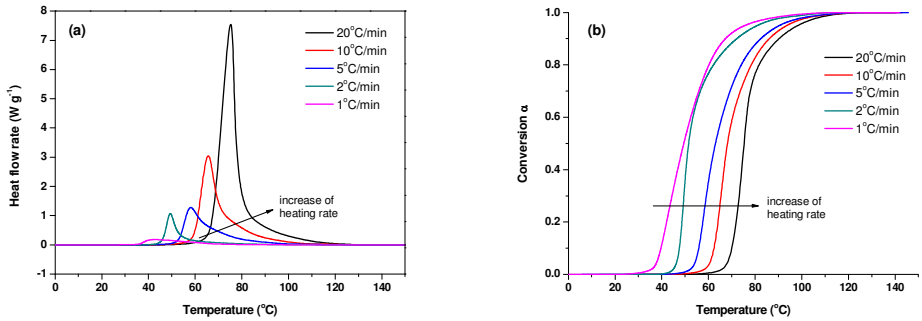


Fig.4.4(a) DSC multiple heating rate method of NCA50-DCPD50;
(b) Plot of conversion as a function of temperature for NCA50-DCPD50

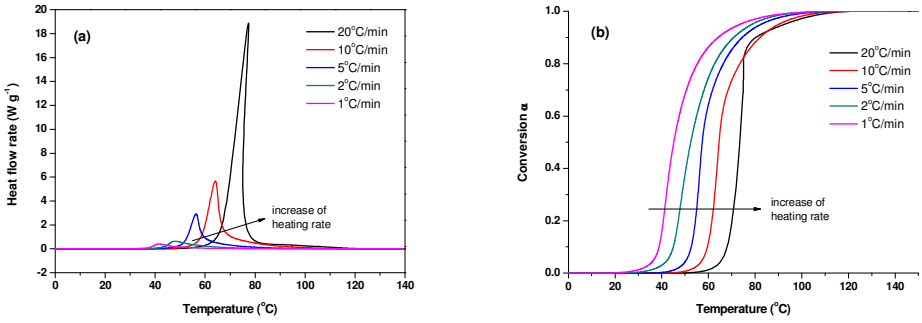


Fig.4.5(a) DSC multiple heating rate method of NCA50-CL50;
(b) Plot of conversion as a function of temperature for NCA50-CL50

The relationship between conversion and temperature at different heating rates can be integrated from the original DSC dynamic scans, shown in Figure 4.4(b) and 4.5(b).

With the same comonomer loading, NCA50-CL50 reaches a given conversion at a lower temperature than NCA50-DCPD50 during dynamic cure, confirming that CL exhibits higher reactivity than DCPD.

The multiple heating rate method is technically identical to model-free kinetics (MFK, Vyazovkin, [44]). Model-free kinetics circumvents using a specific chemical reaction model, such as *n*th-order or autocatalytic. With the set of data from DSC experiments, an isoconversional analysis can be performed to estimate the shift of activation energy $E_a$ over different conversion levels. Compared to model kinetics (often based on isothermal experiments), isoconversional kinetics (using a multiple heating rate method) assume that the activation energy is dependent on conversion rather than a constant value during the cure, and more accurately characterizes the complex changes in reaction mechanism.

Ozawa [45] and Flynn and Wall [46] proposed a simple relationship between activation energy and the heating rate and isoconversion temperature:

$$\log \beta = \frac{-0.4567 E_a}{RT_i} + A' \tag{4.3}$$

Where $\beta = dT/dt$ represents the heating rate, $T_i$ is the isoconversional temperature, $E_a$ is activation energy, and $A'$ is a pre-exponential factor. Conveniently, a linear regression can be drawn based on the experimental plot of $\log \beta$ as a function of $1/T_i$ at each degree of conversion, shown in Figure 4.6(a) and 4.6(b). The activation energy is thus calculated from the slope and the pre-exponential factor $A'$ is obtained from the y-intercept of the

regression. Figure 4.6(c) shows how $E_a$ and $A'$ shift with the increase of conversion α from 10 to 90 %. For both NCA50-DCPD50 and NCA50-CL50 resins, the activation energy increases gradually from a low value (85~87 kJ/mol) over the whole cure. This behavior may be attributed to the diffusion limitation resulting from the formation of a cross-linked network. At the same time, the type of comonomer has an important effect on the change of $E_a$. At the beginning of cure, NCA50-DCPD50 shows a similar $E_a$ as NCA50-CL50. The activation energy gap between CL and DCPD ($E_{a(CL)} < E_{a(DCPD)}$) is compensated by stoichiometric calculation, by which NCA50-CL50 has molar ratio of 76.8% less than 79.9% of NCA50-DCPD50. When the conversion increases above $\alpha$ = 0.6, $E_a$ of NCA50-CL50 surpasses NCA50-DCPD50 and the difference increases up to ~30 kJ/mol at $\alpha$ = 0.9. This can be explained by the fact that CL's higher functionality to ROMP tends to result in higher immobility for the reacting monomers when the cross-linked network develops. The shift of $A'$ is quite similar to the change in $E_a$ with progressing conversion, as was observed in similar studies [42].

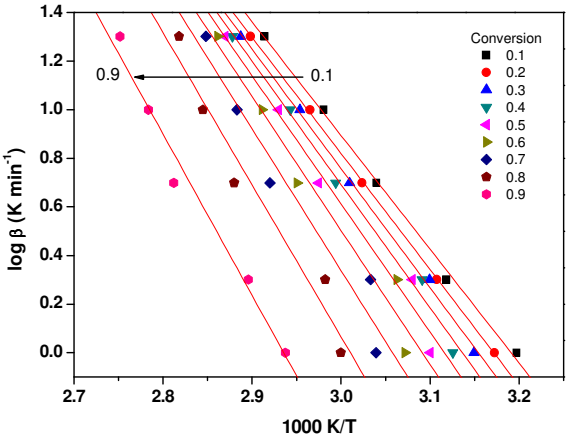


(a)

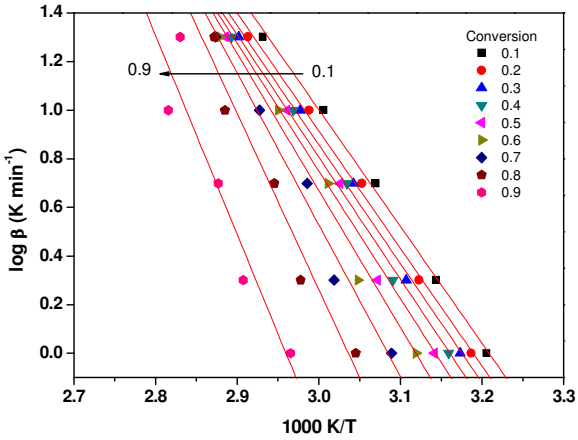


(b)

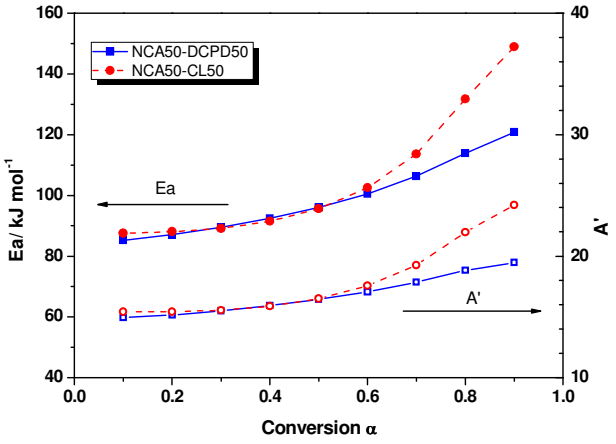


(c)

Fig. 4.6 Isoconversional analysis: Ozawa-Flynn-Wall approach

# Chapter 5: Thermal Mechanical Properties

## 5.1 Glass Transition Temperature

Figure 5.1 shows the evolution of glass transition temperature ($T_g$) as a function of NCA/comonomer ratio. The glass transition temperature of the NCA/comonomer thermosets discussed here was determined by DMA. Initially, DSC was utilized to detect $T_g$ by the heat capacity step, but the change became very ambiguous over the temperature range for oil-predominant copolymers (NCA > 80%) due to the effects of high cross-linking levels and the complex relaxations of oil-based polymer chains [3]. Instead, DMA measurement can clearly identify the glass transition by the sharp decrease in storage modulus ($E'$) and the corresponding peak in dissipation modulus ($E''$) or the damping factor (tan $\delta$). For practical convenience, the maximum value of the tan $\delta$ peak was chosen for the analysis of the glass transition temperature $T_g$.

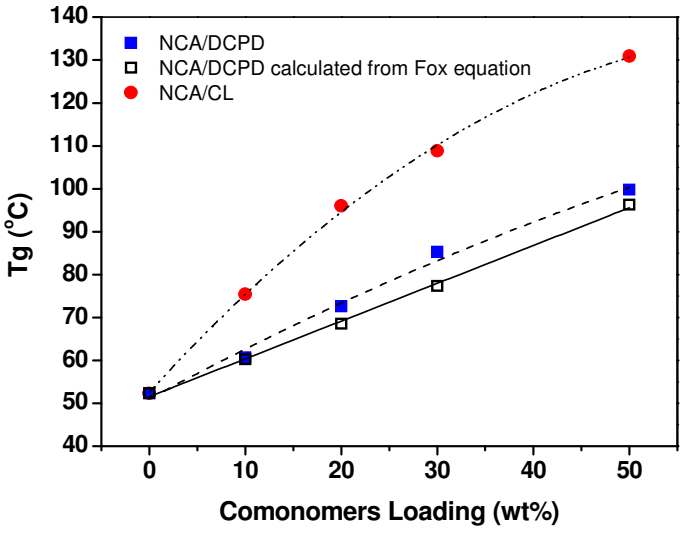


Fig. 5.1 $T_g$ of NCA/DCPD and NCA/CL copolymers as a function of co-monomer loading

From Table 5.1, it is noted that the highest $T_g$ among all samples was below the post-cure temperature of 135 °C. At the same time, the soluble oligomer fraction gained from Soxhlet extraction was less than 1 wt.% for each of the three polymer samples (neat NCA, NCA50-DCPD50, NCA50-CL50). All these data indicated that the NCA/comonomer resins were fully cured using the designed cure schedule.

Table 5.1 Dynamic mechanical properties and cross-link density determined by DMA

| Composition | $T_g$ (°C) | | tan $\delta$ peak | $E'$ at 30 °C (MPa) | $E'$ at $T_g$+50 °C (MPa) | $\nu_e$ (mol/m$^3$) | $M_c$ (g/mol) |
|---|---|---|---|---|---|---|---|
| | by $E''$ peak | by tan $\delta$ peak | | | | | |
| NCA100 | 14.5 | 52.3 | 0.289 | 625 | 51.6 | 2014 | 497 |
| NCA90-DCPD10 | 21.9 | 60.7 | 0.343 | 861 | 46.2 | 1935 | 517 |
| NCA80-DCPD20 | 58.8 | 72.6 | 0.316 | 1159 | 42.4 | 1875 | 533 |
| NCA70-DCPD30 | 72.8 | 85.3 | 0.454 | 1312 | 27.7 | 1573 | 636 |
| NCA50-DCPD50 | 92.4 | 99.8 | 0.538 | 1409 | 23.4 | 1454 | 689 |
| NCA90-CL10 | 48.8 | 75.4 | 0.177 | 1008 | 110.7 | 2554 | 392 |
| NCA80-CL20 | 55.0 | 96.0 | 0.154 | 1310 | 134.1 | 2689 | 372 |
| NCA70-CL30 | 59.6 | 108.8 | 0.144 | 1467 | 122.8 | 2627 | 381 |
| NCA50-CL50 | 110.2 | 130.9 | 0.351 | 1901 | 36.0 | 1759 | 569 |

With increasing co-monomer loading, the glass transition temperatures of NCA/DCPD copolymers ranged from 52.3 to 99.8 °C and that of NCA/CL copolymers ranged from 52.3 to 130.9 °C. The significant shift indicates that the incorporation of DCPD or CL in the macromolecular chains promoted the initiation of cooperative segmental motions at higher temperatures. Similar results have been reported in previous works [4, 7, 13, 47], in which polymerization of the modified linseed oils and DCPD/CL were studied. It is assumed that the increase in $T_g$ is associated with the contribution of the co-monomer's rigid cyclic structure and the effects of higher crosslink densities. In

the following, the influence of different co-monomers on dynamic mechanical behavior, including the glass transition, will be incisively evaluated and compared to the specific castor oil alcohol-based polymer.

In Figure 5.1, the solid square dots indicate the glass transition temperatures of NCA/DCPD copolymers and the solid circles indicate the glass transition temperatures of NCA/CL copolymers obtained from experiments. The two curves display an monotonic increase in glass transition temperatures with an increase in co-monomer loading. The addition of CL results in a higher rate of increase of $T_g$ for the NCA copolymer than adding DCPD. The $T_g$ gap between poly-NCA/CL and poly-NCA/DCPD increases from 14.7 $^oC$ at 10 wt.% to 31.1 $^oC$ at 50 wt.% loading.

The Fox equation provides a simple empirical model to predict the dependence of glass transition temperature on composition in a polymer system, usually in polymer blends and copolymers. The $T_g$ of neat NCA polymer was measured as 52.3 $^oC$ and $T_g$ for poly-DCPD was reported as 153.9 $^oC$ previously [36]; with those two $T_g$s, the $T_g$ of NCA-DCPD copolymers can be calculated as a function of its mass ratio based on the Fox equation, (indicated by the hollow square dots in Figure 5.1):

$$\frac{1}{T_g} = \frac{w_1}{T_{g1}} + \frac{w_2}{T_{g2}} \tag{5.1}$$

Where $T_{g1}$ and $T_{g2}$ represent the glass transition temperatures of poly-NCA and poly-DCPD, respectively (both in Kelvin), $w_1$ and $w_2$ are the corresponding mass fractions. It is clearly seen that the predicted $T_g$ based on the Fox equation deviates from

the experimental $T_g$ for poly-NCA/DCPD. The location of experimental $T_g$ was detected at higher temperatures than the calculated values. Increasing $T_g$ with co-monomer loading differs significantly from the linear relationship that has been reported in related bio-polymers study [10]. However, this non-linear behavior of $T_g$ was also discovered in ROMP thermosets of petroleum-based norbornene derivatives [33]. Comparing those results to ours, a reasonable explanation is that the extent of cross-linking of the polymer system influences the pattern of the shift in $T_g$. Analogous to *endo*-DCPD in Sheng's research [33], the primary component NCA itself was able to form a cross-linked network due to 1.8 of ROMP-reactive norbornene rings per molecule, which is equivalent to a functionality of 3.6 in a vinyl-divinyl system. The incorporation of DCPD and CL, which provide additional multi-functionality, introduces a fluctuation of cross-link density. CL has two norbornene rings of equal reactivity ($f = 4$) and DCPD is able to lightly cross-link due to 20 % of cyclopentene ring opening ($f \approx 2.4$). Once a high level of cross-link density is reached, the mobility between polymer chains may become more limited and free volume for molecule movement is reduced. In the case of Dilulin or norbornene castor oil (NCO)-based polymers, the number of norbornene rings in an oil molecule is approximately 1 on average ($f \approx 2$), which is similar to the bi-functionality of a vinyl monomer. For oil monomers with low cross-linking characteristics the shift in $T_g$ well fit with the Fox equation. Consequently, it appears that the degree of cross-linking distinguishes the $T_g$ shift pattern between multi-functionality copolymerization and bifunctionality copolymerization. The variation in $T_g$'s shift depends on the composition and is determined by the nature of the co-monomers.

## 5.2 Dynamic Mechanical Properties

Figure 5.3(a) and 5.3(b) show the storage modulus ($E'$) and tan $\delta$ as functions of temperature for NCA/DCPD and NCA/CL copolymers with varied mass ratios. Both copolymers displayed a storage modulus at room temperature proportional to comonomer loading. Poly-NCA/DCPD reached the highest $E'$ with 1.4 GPa at 50 % NCA content, while poly-NCA/CL reached storage modulus of up to 1.9 GPa. On the log scale, $E'$ does not appear to be flat prior to the significant decrease even at very low temperature (-50 $^{o}$C) for all the copolymers. The slow decrease of $E'$ in the glassy state may imply a wide band of relaxation below the glass transition. For further discussion of relaxation of cross-linking polymers, data for both $E'$ and tan $\delta$ are needed; this discussion will follow in the next paragraphs. The glass transition region for both polymers is very broad, representing a common characteristic of thermosets. Interestingly, the sharp decrease of $E'$ for NCA/DCPD and NCA/CL copolymers exhibits very different shifts with regard to co-monomer loading. Compared to a more rapid $E'$ decrease in poly-NCA/DCPD, poly-NCA/CL exhibited the decrease in $E'$ by smaller magnitude, as well as over a broader temperature range. Until the highest CL content was reached, the slope of $E'$ unexpectedly resembled the curve for neat poly-NCA.

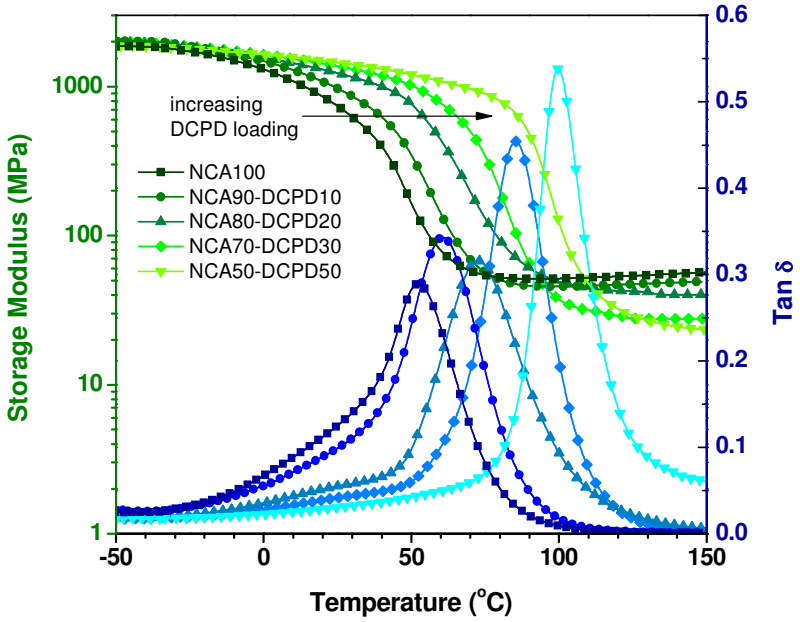


(a)

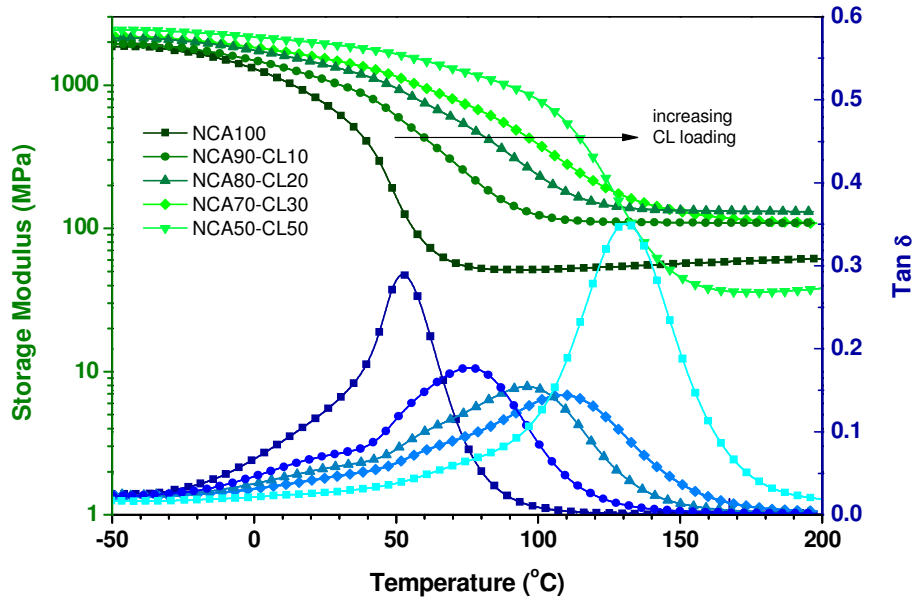


(b)

Fig. 5.3 DMA curves: storage modulus and loss tangent of (a) poly-NCA/DCPD; (b) poly-NCA/CL

Corresponding to the broad decrease of the $E'$ curves, the tan $\delta$ curves were observed to change dissimilarly over the temperature range depending on their composition. All poly-NCA/ DCPD systems, independent of DCPD content, displayed two peaks in the tan $\delta$ spectrum, which is more distinct on the log scale seen in Figure 5.5(b). In the temperature range below where the maximum peak value occurs, a comparable shoulder in damping intensity can be identified for the neat NCA polymer without cross-linking agent. Because poly-NCA is composed of pure NCA monomer, there should be no phase separation in macro scale during polymerization despite the evidence of broad damping peak inferring that inhomogeneity still exists in the network. The maximum peak is normally considered the primary relaxation (α transition), which is often taken as the glass transition. Therefore, it is reasonable to identify the shoulder appearing at a lower temperature as β-transition. The sub-glass transition in the neat NCA polymer occurs near room temperature, indicating a relatively high activity of local segmental motions. Judging from the chemical structure of the poly-NCA main chain, the β-transition is likely linked to crankshaft motions of ester group between the fatty chain and the cyclopentane group, or double bonds in the fatty chain which are illustrated in Figure 5.4.:

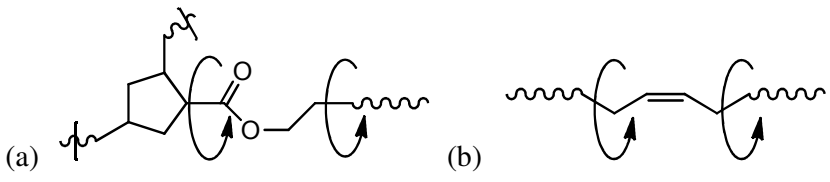


Fig. 5.4 Schematic of crankshaft motions in poly-NCA and its copolymers

Adding DCPD to the poly-NCA decreases the height of the shoulder while the maximum peak becomes larger in intensity and shifts to higher temperatures. A distinct separation between shoulder and peak of tan $\delta$ is observed for the mass ratio of 80/20. With DCPD contents as high as 50%, the shoulder turned out to be almost invisible compared to the primary damping peak. A similar shift can also be discovered in the dissipation curves, illustrated by Figure 5.5(a). This phenomenon may be explained by the fact that the prominence of sub-glass relaxation in poly-NCA/DCPD is reduced by decreasing NCA fraction.

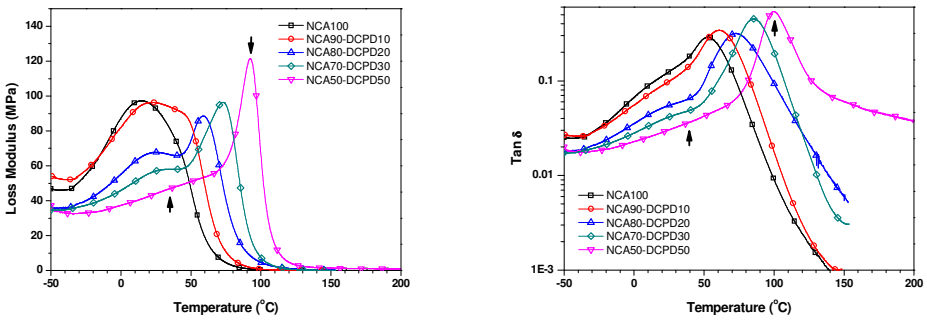


(a) (b)

Fig. 5.5 DMA curves of poly-NCA/DCPD: (a) loss modulus in linear scale; (b) tan $\delta$ in log scale

For poly-NCA/CL systems, the corresponding tan $\delta$ curve shown in Figure 5.6(b) is much more complicated. Firstly, the tan $\delta$ peak occurs over a wider range of temperatures, which almost equal to the entire measurement. This indicates a very complex network structure for thermosets and a high degree of inhomogeneity. Secondly, three shoulders or peaks can be discovered on the tan $\delta$ spectrum as the CL content in the copolymer reaches its highest level. The $E$" curve demonstrate similar three stages within the measured

temperature. Those peaks may be responsible for the different relaxations in the poly-NCA/CL network. Thirdly, other than poly-NCA/DCPD, the maximum damping peak for NCA/CL decreases in height as shifting to higher temperatures with the addition of CL levels lower than 50 %. Surprisingly, at 50 % of CL content, the damping curve increases again, which is consistent with a drop in $E'$ decrease. To better explain the dynamic mechanical behavior of both poly-NCA/CL and poly-NCA/DCPD, it is essential to associate the cross-link density to E' decrease and tan $\delta$ peak and discuss the influence of inhomogeneity of network structure to the thermo-mechanical property.

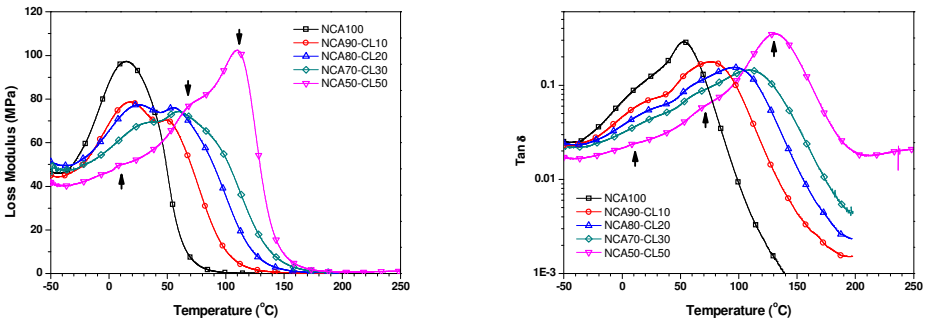


(a) (b)

Fig. 5.6 DMA curves of poly-NCA/CL: (a) loss modulus on linear scale; (b) tan $\delta$ on log scale

## 5.3 The Evaluation of Cross-Link Density

Figures 5.3(a) and 5.3(b) show that at high temperatures above glass transition, copolymers begin to show elastic characteristics, which is designated by the rubbery plateau region. The elastic modulus in the rubbery state is directly due to the contribution of cross-links in the polymer network. In the case of thermosets, cross-links include both chemical cross-links by, in which elastically active network chains (EANC) are

covalently bonded, and physical cross-links created by trapped entanglements. To investigate the effect of cross-link density on dynamic mechanical behavior, the two cross-link types are considered a unified factor for analysis.

The crosslink density ($v_e$) can be determined from the equilibrium shear modulus, which is obtained at $T_g$ + 50 $^oC$ in the rubbery plateau. The kinetic theory of rubber elasticity provides the following relationship [48]:

$$G = \frac{\Phi dRT}{Mc} \qquad \nu_e = \frac{d}{Mc} \tag{5.2}$$

Where Φ is the front factor, normally equaling to 1, $d$ is the density of the polymer, $R$ is the gas constant, and $T$ is the absolute temperature at $T_g$ + 50 $^oC$. $M_c$ is the average molecular weight of EANC between cross-links, which is inversely proportional to the crosslink density $\nu_e$. The equation is only valid for lightly cross-linked rubbers that comply with the assumption of Gaussian chains. It is assumed that Φ is close to unity only when G < 10 MPa [49]. For highly cross-linked polymers, the EANC between two junctions are much shorter and less likely to be randomly curled. It was reported that Equation 5.2 does not give accurate predictions for highly cross-linked polymers such as epoxy and phenol-formaldehyde resins [50].

Therefore, it has been suggested that when elastic shear modulus value exceeds 10 MPa, showing a characteristic of non-Gaussian polymer chains, a modified empirical equation should be used to calculate cross-link density [50]. The equation is given as:

$$\log G = 6 + 23.6 d M_x / M_c \tag{5.3}$$

Where $M_x$ is the molecular weight of the multifunctional cross-linked atoms plus the attached hydrogen atoms. $M_c$ is defined in Equation 5.2. The shear modulus can be substituted by the storage modulus, because for ideal rubber: $G = E'/3$. The density of polymers is unified for the sake of calculation. Cross-link density values and molecular weight between cross-links for both NCA/DCPD and NCA/CL copolymers are listed in Table 5.1..

As can be seen, the cross-link density decreases monotonically with the addition of DCPD, while the value of $M_c$ increases from 497 g/mol to 689 g/mol. It is noteworthy that $T_g$ exhibits a non-linear shift to a higher value with increasing DCPD as mentioned before. It turned out that cross-linking in poly-NCA/DCPD systems did not present a proportional relationship to $T_g$, which is normally seen in thermosets studies. The decrease in cross-link density can be directly related to the difference of multi-functionality in the two components. Because NCA is of higher functionality than DCPD under ROMP, the number of cross-link sites in the copolymer should be reduced with higher amounts of DCPD. On the other aspect, the low cross-linking DCPD has a high $T_g$ mainly because of the rigid structural nature of its polymer backbone. The cyclopentane group, which is the major constitution of ROMP polymers based on norbornene-derivatives, contributes to a very low compliance of chains. The inverse relationship between $T_g$ and cross-link density for the copolymers with DCPD can be explained by the superior effect of structural rigidity compared to the cross-linking. Although DCPD added into the polymer leads to a small decrease in cross-link density, a

more pronounced increase of $T_g$ is achieved when the rigid moiety of DCPD increasingly replaces the flexible aliphatic chains of NCA in the copolymer network.

At a relatively low CL loading (no higher than 30 %), poly-NCA/CL exhibits a typical relationship between cross-link density and dynamic mechanical behavior. As the cross-link density is increased, the glass-to-rubber relaxation diminishes in intensity, broadens, and shifts to higher temperature. The corresponding drop in modulus also decreases in magnitude and expands over a wider temperature range. The trend of increase in $\nu_e$, however, slowed with the addition of CL and reached a top plateau at a CL loading of 20 ~30 wt.%. When the CL content is further increased, up to 50 %, both cross-link density and the DMA curve of poly-NCA/CL reverse, which is indentified by a sharp decrease of storage modulus and a subsequent low value in the rubbery state. An upper limit of the cross-link density that appeared in CL-involved copolymer systems with varied functionalities was noticed but has not yet been investigated in detail. One example was that in a Dilulin-based copolymer, the measured swelling percentage leveled off at a loading level of approx. 40 wt.% of CL [11]. In another example, the effect of CL loading on $\nu_e$ of DCPD-CL copolymers became negligible when CL increased from 15 to 20 wt.% [32]. The reverse change in cross-link density and DMA behavior was not recorded perhaps due to the maximum loading had been achieved for those results. Our result and the previous findings show that the addition of multifunctional cross-linking agent may not always increase the cross-link density of the ROMP thermosetting networks. This improvement takes effect only in a certain low loading levels of CL. To

further increase cross-link density, glass transition temperature, and ambient storage modulus of the ROMP thermosets, it would be necessary to incorporate a specific co-monomer with inherently different chemical structure, for example, higher ROMP functionalities, and polycyclic molecules [51].

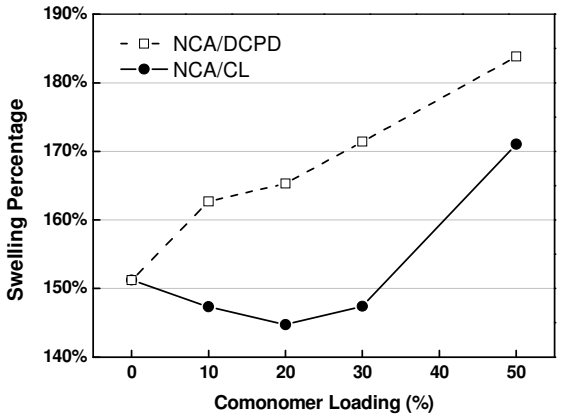


Fig. 5.7 Swelling test of NCA/DCPD and NCA/CL copolymers at various co-monomer loading

## 5.4 Tensile Properties

Figure 5.8 illustrates the stress-strain relationship of NCA/DCPD and NCA/CL copolymers as determined by tensile tests; Young's modulus, tensile strength, strain at break, and toughness are summarized in Table 5.2. Here, two mass ratios (30 and 50 wt.%) of each copolymer were investigated and compared with the neat NCA polymer. The two copolymers exhibited a distinct variation in tensile behavior with the addition of the co-monomer. Neat NCA polymers show ductile behavior and a yield point at about 2 % strain on its stress-strain curve and followed by a plastic deformation region that ended at 12.4 % strain. With low levels of DCPD incorporation, poly-NCA70/DCPD30 exhibited a

considerable improvement in Young's modulus, which increased from 469 to 1213 MPa, as well as in tensile strength, which increased from 15.5 to 28.2 MPa, without detrimental effects on the strain at break. The ductile behavior becomes more remarkable with the sign of a slight decrease in the stress. The incorporation of high levels of DCPD results in poly-NCA50/DCPD50 with the best mechanical properties among the three compositions: Young's modulus of 1699 MPa, tensile strength of 42.9 MPa, and strain at break of 14.0 %. This shift in the stress-strain curve for poly NCA-DCPD is attributed to the predominant effect of creating rigid polymer chains with the incorporation of DCPD , which outweighs the slight decline in cross-linking density.

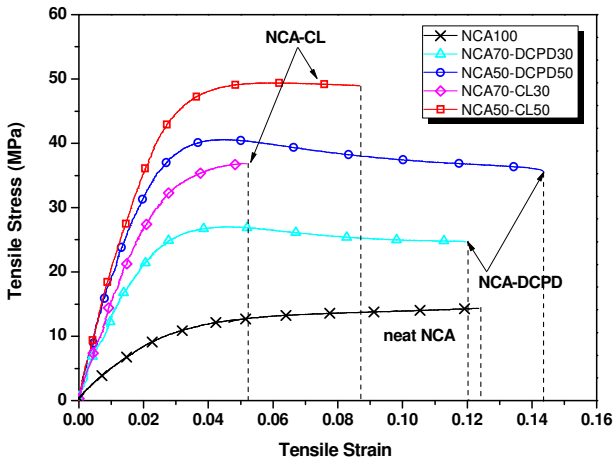


Fig. 5.8 Tensile stress-strain curves of neat NCA, NCA/DCPD, and NCA/CL polymers

Table 5.2 Mechanical properties determined by tensile test

| | E (MPa) | $\sigma_t$ (MPa) | $\varepsilon_b$ (%) | Toughness (J/m$^3$) |
|---|---|---|---|---|
| NCA100 | 469 ± 47 | 15.5 ± 1.4 | 12.4 ± 1.8 | 1.37 ± 0.32 |
| NCA70DCPD30 | 1213 ± 178 | 28.2 ± 0.5 | 11.6 ± 1.9 | 2.66 ± 0.43 |
| NCA50DCPD50 | 1699 ± 428 | 42.9 ± 0.6 | 14.0 ± 1.6 | 4.95 ± 0.55 |
| NCA70CL30 | 1639 ± 259 | 38.9 ± 0.2 | 5.2 ± 0.3 | 1.36 ± 0.10 |
| NCA50CL50 | 2051 ± 128 | 52.2 ± 0.2 | 8.8 ± 0.8 | 3.59 ± 0.40 |

E = Young's modulus, $\sigma_t$ = true stress at maximum tensile strength, $\varepsilon_b$ = true strain at break

With the addition of CL, the copolymer transforms to a brittle behavior at CL loading as high as 30 wt.%. Poly-NCA70/CL30 exhibits the lowest strain at break (5.2 %) and the lowest toughness (1.36 J/m$^3$), which results in poor resistance to rupture. Poly-NCA50/CL50, which had the highest CL loading, displayed an increase in both strain at break $\varepsilon_b$ and in toughness, while Young's modulus *E* and tensile strength $\sigma_t$ continuously improved. The shift pattern is associated with the variation of cross-link density in the NCA/CL copolymer system. The increase or decrease of cross-link density controls the mechanical behavior of the material to a large extent. Last but not least, independently of which cross-linking agent was added, Young's modulus and tensile strength of the NCA copolymers significantly increased. Similar to the effect on glass transition temperature, CL also improves the mechanical properties to a higher degree than DCPD.

## 5.5 Thermal Stability

Thermogravimetric analysis results for both NCA/DCPD and NCA/CL copolymers are shown in Figure 5.9(a) and 5.9(b). The temperature at weight loss values of 5 %, 10 %

and maximum rate of weight loss are chosen to evaluate the thermal stability of the thermosets listed in Table 5.3. With the help of the weight loss derivative, the TGA curves for all copolymers can be divided into three stages. The first stage represents a slow decline over the temperature range from 250 to 400 $^{o}$C, which may be related to the decomposition of side chains or branches that are lightly cross-linked within the thermosetting network. Soluble fractions or unreacted monomers may not be a influencing factor to this stage because the extraction results confirmed that the resins were fully cured. The second stage ranging from 400 to 500 $^{o}$C corresponds to a significant collapse in weight percentage. During this stage, the thermosets are subjected to fast decomposition of main chains in the network, e.g., the cleavage of C=C bonds and ester groups. The third stage, which extends to 650 $^{o}$C, is responsible for the oxidation of residual char from the last stage.

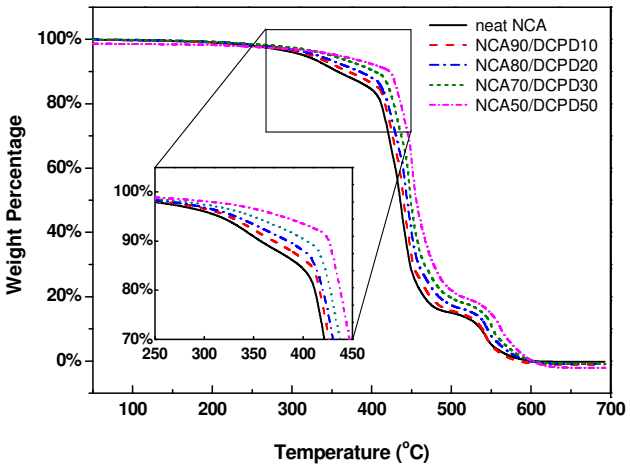


(a)

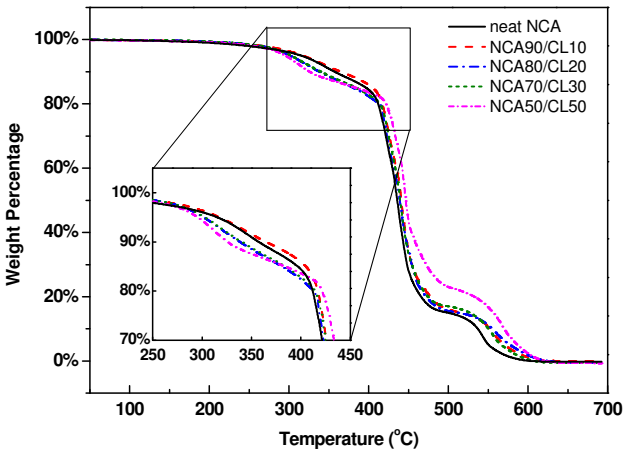


(b)

Fig. 5.9 TGA curves of (a) NCA/DCPD and (b) NCA/CL copolymers

Table 5.3 TGA data of NCA/DCPD and NCA/CL copolymers

| **Composition** | $T_5$ [a] (°C) | $T_{10}$ [b] (°C) | $T_{max}$ [c] (°C) |
|---|---|---|---|
| NCA100 | 315 | 357 | 435 |
| NCA90-DCPD10 | 325 | 370 | 440 |
| NCA80-DCPD20 | 332 | 385 | 444 |
| NCA70-DCPD30 | 349 | 404 | 447 |
| NCA50-DCPD50 | 379 | 426 | 451.5 |
| NCA90-CL10 | 317 | 365 | 442 |
| NCA80-CL20 | 301 | 338 | 440 |
| NCA70-CL30 | 302 | 340 | 441 |
| NCA50-CL50 | 295 | 325 | 440 |

[a] Temperature at 5 % weight loss

[b] Temperature at 10 % weight loss

[c] Temperature at maximum rate of thermal degradation

As shown in Figure 5.9(a), for all three stages the weight loss curve is elevated with the increase of DCPD loading in poly-NCA/DCPD. This consistent shift is also seen in the increasing value of $T_5$, $T_{10}$ and $T_{max}$ in Table 5.3. The data show that DCPD contributes superior thermal stability to the bio-based NCA polymer. Figure 5.9(b) shows

that poly-NCA/CL does not exhibit the same characteristic shift with CL loading as poly-NCA/DCPD. The slope of the weight loss curve for poly-NCA/CL decreases in the first stage, as illustrated in the enlarged picture. This can be explained by the existence of more pronounced heterogeneity in the poly-NCA/CL network. In thermosetting structures with high CL loadings, the higher number of branches that are loosely connected to the main chains may be susceptible to debonding and oxidization at elevated temperatures. The degradation resistance of NCA-CL copolymers is limited due to the network heterogeneity.

# Chapter 6: General Conclusions

Norbornenyl-functionalized castor oil alcohol (NCA) was successfully synthesized using a modified approach. NCA was cured with either DCPD or cross-linker by ROMP using 2nd generation Grubbs' catalysts and formed a variety of thermosets.

Isothermal kinetic DSC methods show that NCA-DCPD and NCA-CL resins behave similarly at maximum conversion rates. The cure temperature affected conversion rates to a large extent. The time until maximum conversion and the value of the maximum conversion rate indicate that CL reacts faster than DCPD during the ROMP-based cure of NCA resin. The fact that both resins reach 90 % of conversion in just 5 min at 70 $^{o}$C indicates the high efficiency of ROMP cure in the system. With the kinetic information provided by isothermal curing, 60 $^{o}$C is chosen as the cure temperature for the overall compositions and post-curing at 135 $^{o}$C guarantees full conversion.

The appearance of a single exothermic peak in DSC dynamic scans indicates the simple reaction mechanism of ROMP between NCA and the cross-linking agents. For the same mass fraction, NCA-CL resins released a larger amount of the total reaction heat $\Delta H_{rxn}$ than NCA-DCPD resins during cure. The relationship between conversion and temperature at different heating rates shows that CL exhibits higher reactivity compared to DCPD. Using Ozawa-Flynn-Wall analysis it was shown that the calculated activation energy increases during the entire curing process for both resins. The shift pattern is related to the diffusion limitation and the difference in co-monomer functionalities in the cross-linked network.

DMA results showed that the glass transition temperatures of poly-NCA/DCPD and poly-NCA/CL increased with the addition of co-monomers. The curve of $T_g$ vs. DCPD loading for poly-NCA/DCPD was not well described by the Fox equation because of the high level of cross-linking originated from the multi-functionality of NCA-DCPD. Storage modulus at room temperature of both copolymers increased significantly. The sharp decrease of $E'$ in glass transition and the corresponding damping peak indicate very different shifts for poly-NCA/DCPD and poly-NCA/CL caused by the addition of co-monomers. Poly-NCA/DCPD systems displayed two peaks on the tan $\delta$ curves that are related to the primary transition and the secondary transition. The cross-link density calculated by a new empirical equation slightly decreased with increasing DCPD loading. Poly-NCA/CL systems exhibited three shoulders in the broad damping peak, indicating a complicated network structure. It was found that the cross-link density could reverse with increasing loading levels of CL.

The stress-strain relationship of NCA/DCPD and NCA/CL copolymers determined by tensile test showed a general increase in Young's modulus and tensile strength, but a distinct pattern of shift in strain at break and toughness. The incorporation of DCPD renders NCA copolymer more ductile and strong. The structure rigidity of DCPD has a more dominant influence than cross-linking in poly NCA/DCPD systems. Brittle behavior was observed in poly-NCA/CL with low CL loading levels, while high CL loading levels led to ductile behavior. The continuous increase of Young's modulus and tensile strength was attributed to CL's rigid nature and the reversal of toughness was related to the

cross-link density.

TGA of poly-NCA/DCPD indicated a constant increase for all stages of weight loss curve and poly-NCA/CL does not exhibit similar shifts with the increase of co-monomer loading. The discrepancy may be the result of the more significant heterogeneity in the poly-NCA/CL network.

# Reference


1. Li, F.K. and R.C. Larock, *Thermosetting polymers from cationic copolymerization of tung oil: Synthesis and characterization.* Journal of Applied Polymer Science, 2000. **78**(5): p. 1044-1056.
2. Li, F.K. and R.C. Larock, *Synthesis, structure and properties of new tung oil-styrene-divinylbenzene copolymers prepared by thermal polymerization.* Biomacromolecules, 2003. **4**(4): p. 1018-1025.
3. Can, E., R.P. Wool, and S. Kusefoglu, *Soybean and castor oil based monomers: Synthesis and copolymerization with styrene.* Journal of Applied Polymer Science, 2006. **102**(3): p. 2433-2447.
4. Henna, P. and R.C. Larock, *Novel Thermosets Obtained by the Ring-Opening Metathesis Polymerization of a Functionalized Vegetable Oil and Dicyclopentadiene.* Journal of Applied Polymer Science, 2009. **112**(3): p. 1788-1797.
5. Andjelkovic, D.D., et al., *Novel Rubbers from the Cationic Copolymerization of Soybean Oils and Dicyclopentadiene, 2-Mechanical and Damping Properties.* Macromolecular Materials and Engineering, 2009. **294**(8): p. 472-483.
6. Andjelkovic, D.D. and R.C. Larock, *Novel rubbers from cationic copolymerization of soybean oils and dicyclopentadiene. 1. Synthesis and characterization.* Biomacromolecules, 2006. **7**(3): p. 927-936.
7. Andjelkovic, D.D. and R. Larock, *Mechanical properties of novel rubbers from the cationic copolymerization of soybean oil and dicyclopentadiene.* Abstracts of Papers of the American Chemical Society, 2006. **231**.
8. Andjelkovic, D.D., et al., *Novel thermosets prepared by cationic copolymerization of various vegetable oils - synthesis and their structure-property relationships.* Polymer, 2005. **46**(23): p. 9674-9685.
9. Xia, Y., Y.S. Lu, and R.C. Larock, *Ring-opening metathesis polymerization (ROMP) of norbornenyl-functionalized fatty alcohols.* Polymer, 2010. **51**(1): p. 53-61.
10. Xia, Y. and R.C. Larock, *Castor oil-based thermosets with varied crosslink densities prepared by ring-opening metathesis polymerization (ROMP).* Polymer, 2010. **51**(12): p. 2508-2514.
11. Jeong, W., et al., *Bio-Based Rubbers by Concurrent Cationic and Ring-Opening Metathesis Polymerization of a Modified Linseed Oil.* Macromolecular Materials and Engineering, 2009. **294**(11): p. 756-761.
12. Badrinarayanan, P., et al., *Cure Characterization of Soybean Oil-Styrene-Divinylbenzene Thermosetting Copolymers.* Journal of Applied Polymer Science, 2009. **113**(2): p. 1042-1049.
13. Mauldin, T.C., et al., *Ring-Opening Metathesis Polymerization of a Modified Linseed Oil with Varying Levels of Crosslinking*. Journal of Polymer Science Part a-Polymer Chemistry, 2008. **46**(20): p. 6851-6860.
14. Kundu, P.P. and R.C. Larock, *Novel conjugated linseed oil-styrene-divinylbenzene copolymers prepared by thermal polymerization. 1. Effect of monomer concentration on the structure and properties.* Biomacromolecules, 2005. **6**(2): p. 797-806.
15. Li, F.K., J. Hasjim, and R.C. Larock, *Synthesis, structure, and thermophysical and mechanical properties of new polymers prepared by the cationic copolymerization of corn oil, styrene, and divinylbenzene.* Journal of Applied Polymer Science, 2003. **90**(7): p. 1830-1838.
16. Calderon, N., *Ring-Opening Polymerization of Cycloolefins.* Journal of Macromolecular

Science-Reviews in Macromolecular Chemistry and Physics, 1972. **C 7**(1): p. 105-&.

17. Calderon, N., *Olefin Metathesis Reaction.* Accounts of Chemical Research, 1972. **5**(4): p. 127-&.
18. Benson, S.W., et al., *Additivity Rules for Estimation of Thermochemical Properties.* Chemical Reviews, 1969. **69**(3): p. 279-&.
19. Ho, S.C.H., D.A. Straus, and R.H. Grubbs, *An Alternate Path to Reductive Elimination for Group 4b Metals - Mechanism of Cyclopropane Formation from Titanacyclobutanes.* Journal of the American Chemical Society, 1984. **106**(5): p. 1533-1534.
20. Trnka, T.M. and R.H. Grubbs, *The development of L2X2Ru = CHR olefin metathesis catalysts: An organometallic success story.* Accounts of Chemical Research, 2001. **34**(1): p. 18-29.
21. Leitgeb, A., J. Wappel, and C. Slugovc, *The ROMP toolbox upgraded.* Polymer, 2010. **51**(14): p. 2927-2946.
22. Grubbs, R.H., *Olefin-metathesis catalysts for the preparation of molecules and materials (Nobel lecture).* Angewandte Chemie-International Edition, 2006. **45**(23): p. 3760-3765.
23. Grubbs, R.H. and W. Tumas, *Polymer Synthesis and Organotransition Metal Chemistry.* Science, 1989. **243**(4893): p. 907-915.
24. Rouhi, A.M., *Olefin metathesis: Big-deal reaction.* Chemical & Engineering News, 2002. **80**(51): p. 29-33.
25. Rouhi, A.M., *Olefin metathesis: The early days.* Chemical & Engineering News, 2002. **80**(51): p. 34-38.
26. White, S.R., et al., *Autonomic healing of polymer composites (vol 409, pg 794, 2001).* Nature, 2002. **415**(6873): p. 817-817.
27. Rule, J.D. and J.S. Moore, *ROMP reactivity of endo- and exo-dicyclopentadiene.* Macromolecules, 2002. **35**(21): p. 7878-7882.
28. Mauldin, T.C., et al., *Self-healing kinetics and the stereoisomers of dicyclopentadiene.* Journal of the Royal Society Interface, 2007. **4**(13): p. 389-393.
29. Lee, J.K., et al., *Characterization of dicyclopentadiene and 5-ethylidene-2-norbornene as self-healing agents for polymer composite and its microcapsules.* Macromolecular Research, 2004. **12**(5): p. 478-483.
30. Lee, J.K., et al., *Thermal analysis of ring-opening metathesis polymerized healing agents.* Journal of Polymer Science Part B-Polymer Physics, 2007. **45**(14): p. 1771-1780.
31. Mauldin, T.C. and M.R. Kessler, *Enhanced bulk catalyst dissolution for self-healing materials.* Journal of Materials Chemistry, 2010. **20**(20): p. 4198-4206.
32. Liu, X., et al., *Rheokinetic evaluation of self-healing agents polymerized by Grubbs catalyst embedded in various thermosetting systems.* Composites Science and Technology, 2009. **69**(13): p. 2102-2107.
33. Sheng, X., M.R. Kessler, and J.K. Lee, *The influence of cross-linking agents on ring-opening metathesis polymerized thermosets.* Journal of Thermal Analysis and Calorimetry, 2007. **89**(2): p. 459-464.
34. Sheng, X., J.K. Lee, and M.R. Kessler, *Influence of cross-link density on the properties of ROMP thermosets.* Polymer, 2009. **50**(5): p. 1264-1269.
35. Jeong, W. and M.R. Kessler, *Effect of functionalized MWCNTs on the thermo-mechanical properties of poly(5-ethylidene-2-norbornene) composites produced by ring-opening metathesis polymerization.* Carbon, 2009. **47**(10): p. 2406-2412.

36. Jeong, W. and M.R. Kessler, *Toughness Enhancement in ROMP Functionalized Carbon Nanotube/Polydicyclopentadiene Composites.* Chemistry of Materials, 2008. **20**(22): p. 7060-7068.
37. Chen, J.X., et al., *Synthesis and photopolymerization of norbornyl epoxidized linseed oil.* Polymer, 2002. **43**(20): p. 5379-5389.
38. Henna, P.H., M.R. Kessler, and R.C. Larock, *Fabrication and Properties of Vegetable-Oil-Based Glass Fiber Composites by Ring-Opening Metathesis Polymerization.* Macromolecular Materials and Engineering, 2008. **293**(12): p. 979-990.
39. Qiao, R.R., C.H. Yang, and M.Y. Gao, *Superparamagnetic iron oxide nanoparticles: from preparations to in vivo MRI applications (vol 19, pg 6274, 2009).* Journal of Materials Chemistry, 2009. **19**(48): p. 9286-9286.
40. Stille, J.K. and D.A. Frey, *Tetracyclic Dienes .1. The Diels-Alder Adduct of Norbornadiene and Cyclopentadiene.* Journal of the American Chemical Society, 1959. **81**(16): p. 4273-4275.
41. Jones, A.S., et al., *Catalyst morphology and dissolution kinetics of self-healing polymers.* Chemistry of Materials, 2006. **18**(5): p. 1312-1317.
42. Kessler, M.R. and S.R. White, *Cure kinetics of the ring-opening metathesis polymerization of dicyclopentadiene.* Journal of Polymer Science Part a-Polymer Chemistry, 2002. **40**(14): p. 2373-2383.
43. Haman, K., P. Badrinarayanan, and M.R. Kessler, *Cure characterization of the ring-opening metathesis polymerization of linseed oil-based thermosetting resins.* Polymer International, 2009. **58**(7): p. 738-744.
44. Vyazovkin, S., *A unified approach to kinetic processing of nonisothermal data.* International Journal of Chemical Kinetics, 1996. **28**(2): p. 95-101.
45. Ozawa, T., *A New Method of Analyzing Thermogravimetric Data.* Bulletin of the Chemical Society of Japan, 1965. **38**(11): p. 1881-&.
46. Flynn, J.H. and L.A. Wall, *A Quick Direct Method for Determination of Activation Energy from Thermogravimetric Data.* Journal of Polymer Science Part B-Polymer Letters, 1966. **4**(5pb): p. 323-&.
47. Xia, Y., P.H. Henna, and R.C. Larock, *Novel Thermosets from the Cationic Copolymerization of Modified Linseed Oils and Dicyclopentadiene.* Macromolecular Materials and Engineering, 2009. **294**(9): p. 590-598.
48. Levita, G., et al., *Cross-Link Density and Fracture-Toughness of Epoxy-Resins.* Journal of Materials Science, 1991. **26**(9): p. 2348-2352.
49. Tobolsky, A.V., et al., *Rubber Elasticity in Highly Crosslinked Systems - Crosslinked Styrene Methyl Methacrylate Ethyl Acrylate + Octyl Acrylate.* Journal of Polymer Science Part a-General Papers, 1964. **2**(6pa): p. 2749-&.
50. Nielsen, L.E., *Cross-Linking-Effect on Physical Properties of Polymers.* Journal of Macromolecular Science-Reviews in Macromolecular Chemistry, 1969. **C 3**(1): p. 69-&.
51. Keck, C.G., J.L. Kendall, and K.C. Caster, *Cross-linkers for improved high temperature performance of ROMP adhesives.* Advanced Synthesis & Catalysis, 2007. **349**(1-2): p. 165-174.